forests

MDPI

Article

Spatial Structure Evaluation of Chinese Fir Plantation in Hilly Area of Southern China Based on UAV and Cloud Model

Jinyan Liu [1,2], Bowen Jin [2], Guochang Ding [2], Xiang Huang [3,*] and Jianwen Dong [2,*]

[1] College of Resource and Environmental Sciences, Quanzhou Normal University, 398 Donghai Rd., Quanzhou 362000, China; fjljy@qztc.edu.cn
[2] College of Landscape Architecture and Art, Fujian Agriculture and Forestry University, 63 Xiyuangong Rd., Fuzhou 350002, China; 62419052012@fafu.edu.cn (B.J.); fjdgc@fafu.edu.cn (G.D.)
[3] College of Forestry, Fujian Agriculture and Forestry University, Fuzhou 350002, China
* Correspondence: 22404030006@fafu.edu.cn (X.H.); fjdjw@fafu.edu.cn (J.D.); Tel.: +86-132-3590-5585 (X.H.); +86-136-0952-5156 (J.D.)

Abstract

Chinese fir, as a crucial fast-growing tree species in the hilly regions of southern China, exhibits spatial structure characteristics that directly influence both the ecological functionality and productivity of its stands. This study focused on Chinese fir plantations in the Yangkou State-Owned Forest Farm, Fujian Province. Using UAV-LiDAR point cloud data, individual tree parameters such as height and crown width were extracted, and a DBH inversion model was constructed by integrating machine learning algorithms. Spatial structure parameters were quantified through weighted Voronoi diagrams. A comprehensive evaluation system was established based on the combined weighting method and fuzzy evaluation model to systematically analyze spatial structure characteristics and their evolutionary patterns across different age classes. The results demonstrated that growth environment indicators (openness and openness ratio) progressively declined with the stand's age, reflecting deteriorating light conditions due to increasing canopy closure. Growth superiority (size ratio and angle competition index) exhibited a "V"-shaped trend, with the most intense competition occurring in the middle-aged stands before stabilizing in the over-mature stage. The resource utilization efficiency (uniform angle and forest layer index) showed continuous optimization, reaching optimal spatial configuration in over-mature stands. This study developed a spatial structure evaluation system for Chinese fir plantations by combining UAV data and cloud modeling, elucidating structural characteristics and developmental patterns across different growth stages, thereby providing theoretical foundations and technical support for close-to-nature management and the precision quality improvement of Chinese fir plantations.

Keywords: UAV-LiDAR; Chinese fir plantation; spatial structure of stands; cloud model theory

check for updates

Academic Editor: Eric Casella

Received: 31 July 2025
Revised: 27 August 2025
Accepted: 16 September 2025
Published: 18 September 2025

Citation: Liu, J.; Jin, B.; Ding, G.; Huang, X.; Dong, J. Spatial Structure Evaluation of Chinese Fir Plantation in Hilly Area of Southern China Based on UAV and Cloud Model. *Forests* **2025**, *16*, 1483. https://doi.org/10.3390/f16091483

Copyright: © 2025 by the authors. Licensee MDPI, Basel, Switzerland. This article is an open access article distributed under the terms and conditions of the Creative Commons Attribution (CC BY) license (https://creativecommons.org/licenses/by/4.0/).

1. Introduction

Chinese fir (*Cunninghamia lanceolata*), as one of the most important fast-growing timber species in the hilly regions of southern China, plays a vital role in plantation establishment and timber supply [1,2]. However, long-term management practices focusing primarily on timber production, characterized by short rotation periods and insufficient structural regulation, have led to degradation trends in stand structure, functionality, and ecological stability [3–5]. Therefore, optimizing the ecological and productive functions of Chinese fir

plantations through scientific management has become a crucial issue in current forestry research and practice.

Stand spatial structure, as a readily manageable and regulable factor, serves as the fundamental basis for optimizing silvicultural practices. It characterizes the spatial distribution patterns and interrelationships among individual trees and their components within three-dimensional space [6–9]. The rationality of spatial structure not only directly determines stand efficiency in acquiring essential resources such as light, water, and nutrients, but also governs competitive dynamics within plant communities and their resilience to disturbances [10–13]. Numerous studies have demonstrated that structurally optimized stands exhibit superior resource utilization efficiency, enhanced ecological stability, and improved stress resistance [14,15]. To elucidate the structure–function relationships in forest ecosystems, researchers worldwide have developed various quantitative indicator systems for spatial structure analysis, including horizontal structure descriptors (e.g., uniform angle, size ratio, and angle competition index) [16–18] and vertical structure parameters (e.g., forest layer index and openness) [19,20], which collectively provide a theoretical foundation for comprehensive structural characterization. These indicators not only reveal the spatial heterogeneity within stands but also offer quantitative benchmarks for structural regulation in forest management practices.

However, the analysis and evaluation of stand spatial structure has always been a focus in sustainable forest management worldwide. Traditional spatial structure analysis mainly relies on multiple single-factor analyses [21,22]. While this approach has advantages such as mature calculation methods and operational simplicity, facilitating the understanding of certain aspects of stand structure, it overlooks the correlations among structural factors and struggles to comprehensively reflect the overall structural status of stands. Moreover, the lack of a weighting system makes it difficult to form unified comprehensive evaluation results, limiting its application potential in precision management and intelligent operations. The homogeneity evaluation of stand spatial structures based on multiplication–division principles or comprehensive index evaluation methods represents a breakthrough from traditional approaches by incorporating multiple indicators for a comprehensive assessment [23,24]. However, these methods do not consider the relative importance of different indicators on stand spatial structure and rely solely on optimization through maximization or minimization in calculations, resulting in certain scientific limitations in their evaluation outcomes. Furthermore, whether using single-factor or multi-factor evaluation methods, the calculation of stand spatial structure parameters requires the manual collection of plot data, consuming significant human and material resources. Therefore, how to efficiently and accurately obtain stand structure data and conduct scientific evaluations has become an urgent issue to address for achieving efficient forest management.

With the advancement of remote sensing technologies, particularly the application of low-altitude UAV-LiDAR in forestry, new possibilities have emerged for the efficient acquisition and quantitative analysis of stand spatial structure [25]. Compared to traditional ground-based measurement methods, high-altitude spacecraft remote sensing, and satellite remote sensing, UAV platforms offer distinct advantages including superior operational flexibility, high data resolution, and cost-effectiveness [26], enabling the rapid acquisition of three-dimensional point cloud data over large forest areas, thereby establishing a technical foundation for extracting and analyzing structural parameters at the individual tree level. In the past, it was necessary to measure the basic parameters of trees and their relative position information in the sample plot manually in the process of extracting forest spatial structure parameters, which is not only time-consuming and laborious, but also uncertain. According to the research of relevant scholars, UAV lidar can accurately identify the spatial position, canopy shape, tree height, canopy width, and other structural characteristics of

trees, significantly improving the description accuracy of forest structure [27–30]. Under this background, this study took the Chinese fir plantation in Fujian Province as the object, and integrated UAV remote sensing and game theory–cloud model theory to construct the evaluation system of stand spatial structures. By extracting spatial parameters of the individual tree and stand, the evolution law of structure with forest age was revealed, and a quantitative evaluation method was established, which provided technical support for the precise management and sustainable management of Chinese fir plantation.

2. Materials and Methods

2.1. Study Area

This study was conducted in Chinese fir plantations at the Yangkou State-Owned Forest Farm in Shunchang County, Nanping City, Fujian Province. The forest farm is situated on the southeastern foothills of the Wuyi Mountains (117°29′~118°14′ E, 26°38′~27°12′ N), within the mid-subtropical monsoon climate zone (Figure 1). The region enjoys favorable hydrothermal conditions, with mean annual temperatures ranging from 18 to 20 °C and annual precipitation between 1600 and 1800 mm [31,32]. The study area includes Chinese fir stands at different developmental stages: young forest, middle-aged forest, near-ripe forest, mature forest, and overripe forest. As an important Chinese fir cultivation base in southern China, the structural evolution patterns of stands in Yangkou Forest Farm provide significant reference value for sustainable management of regional plantations.

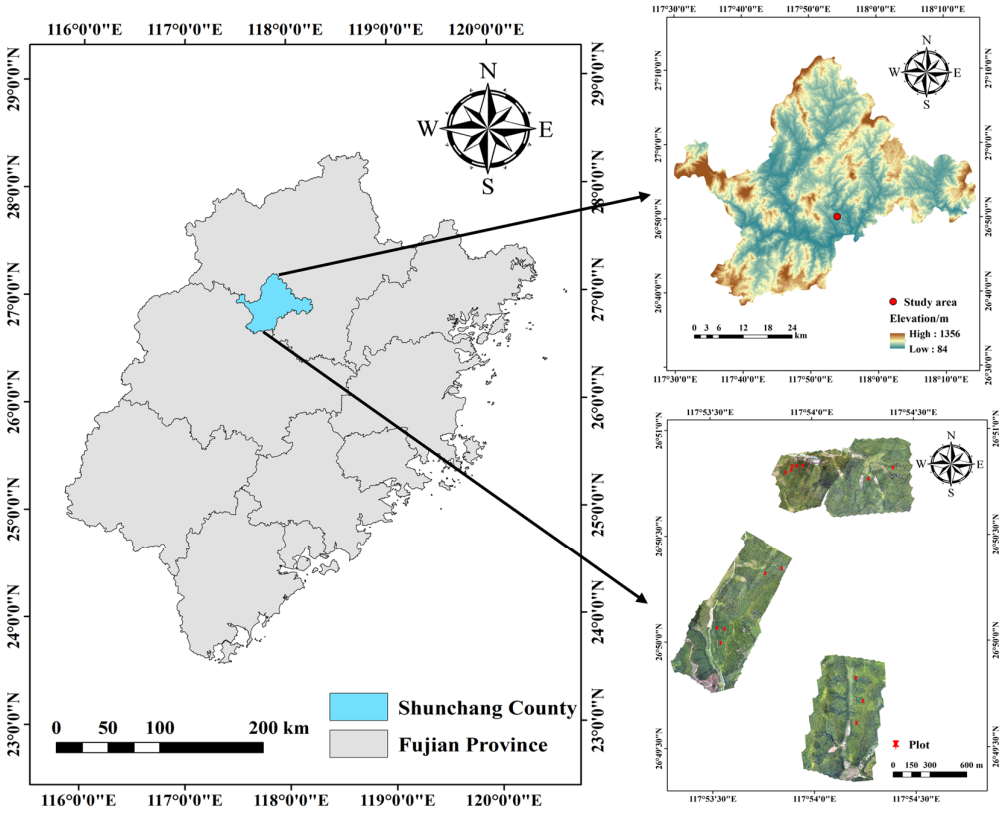

Figure 1. Overview map of the study area.

2.2. Data Acquisition

Field data collection and surveys were conducted in August 2022. The selection of sample plots encompassed young forest, middle-aged forest, near-ripe forest, mature forest, and overripe forest, with three replicates established for each age group, totaling 15 sample plots (25.82 m × 25.82 m). In the process of sample plot selection, first we ensure that there

is no large difference in natural conditions such as slope and altitude, and then we divide it into 5 levels according to the difference in the forest age of the fir plantation in the study area, corresponding to different age groups, and completely randomly select 3 sample plots in different age groups to ensure that the probability of each sample plot being selected is equal, and finally, a total of 15 representative sample plots are selected. The ground survey data included tree height, crown width, diameter at breast height (DBH), stand density, canopy closure, as well as slope and elevation. Additionally, approximately 10 trees were randomly selected from each plot for RTK (Real-Time Kinematic) positioning, totaling 153 trees used for accuracy validation of UAV parameter extraction results and construction of the Chinese fir individual tree DBH model. The survey results are presented in Table 1.

Table 1. Sample plot survey information form.

Age Group	Average Tree Height/m	Average DBH/cm	Average CW/m	Stand Density Trees/ha	Canopy Closure	Slope/°	Elevation/m
Young forest	9.1 ± 0.8	12.2 ± 1.5	2.4 ± 0.2	2533.7 ± 320.6	0.8 ± 0.02	23.0 ± 3.5	220.7 ± 8.1
Middle-aged forest	13.2 ± 1.0	15.3 ± 1.8	2.8 ± 0.1	1244.4 ± 128.1	0.6 ± 0.06	26.7 ± 5.1	195.7 ± 6.5
Near-ripe forest	15.7 ± 1.5	17.6 ± 1.0	3.0 ± 0.1	2203.9 ± 166.9	0.8 ± 0.11	25.0 ± 1.0	212.3 ± 13.3
Mature forest	17.3 ± 1.5	22.8 ± 2.4	3.2 ± 0.2	914.5 ± 368.1	0.6 ± 0.10	26.0 ± 1.2	227.0 ± 32.6
Overripe forest	19.3 ± 1.9	25.9 ± 2.6	3.6 ± 0.1	1289.4 ± 550.4	0.7 ± 0.07	27.7 ± 2.8	208.3 ± 5.7

UAV point cloud data acquisition was conducted simultaneously with the ground surveys. The Feima D500 UAV, equipped with a HESAI XT32 sensor, was used to obtain point cloud data for each sample plot. As the study area is located in a typical hilly region with significant terrain undulations, the data acquisition scheme adopted was as follows: terrain-following flight at 150 m altitude, 80% laser side overlap rate, and the laser operating in triple-echo mode.

2.3. Method

2.3.1. Extraction of Single-Tree Parameters

(1) Single-tree segmentation with CHM (Canopy Height Model) and point cloud

The CHM-based single-tree segmentation method primarily considers the two-dimensional aspects of images, potentially overlooking smaller trees in the forest, thereby impacting segmentation outcomes [33]. Conversely, the single-tree segmentation approach based on point cloud data leverages the benefits of three-dimensional data, offering a more accurate representation of forest conditions. Nonetheless, this method's segmentation results are highly sensitive to parameter settings, elevating the complexity of forest data processing [34]. To address these limitations, we investigated a hybrid single-tree segmentation approach that integrates CHM and point cloud data; Figure 2 shows the flow chart of single tree segmentation:

① Normalize the elevation of point cloud data, then use cloth filtering algorithm to separate ground points and non-ground points, transform the two kinds of point clouds into raster data by ArcGIS 10.8, generate DEM (Digital Elevation Model, 0.1 m × 0.1 m) and DSM (Digital Surface Model, 0.1 m × 0.1 m), respectively, and finally, use raster calculation tools to make DSM and DEM difference to CHM (0.1 m × 0.1 m).

② Gaussian smoothing filter is performed on the generated CHM to eliminate high-frequency noise in the CHM and make the data more continuous. Morphological closing filling is performed on the smoothed CHM, which is used to fill in local depressions caused by missing data or low vegetation in CHM, ensure that the crown area is more complete, and improve the accuracy of single-tree detection.

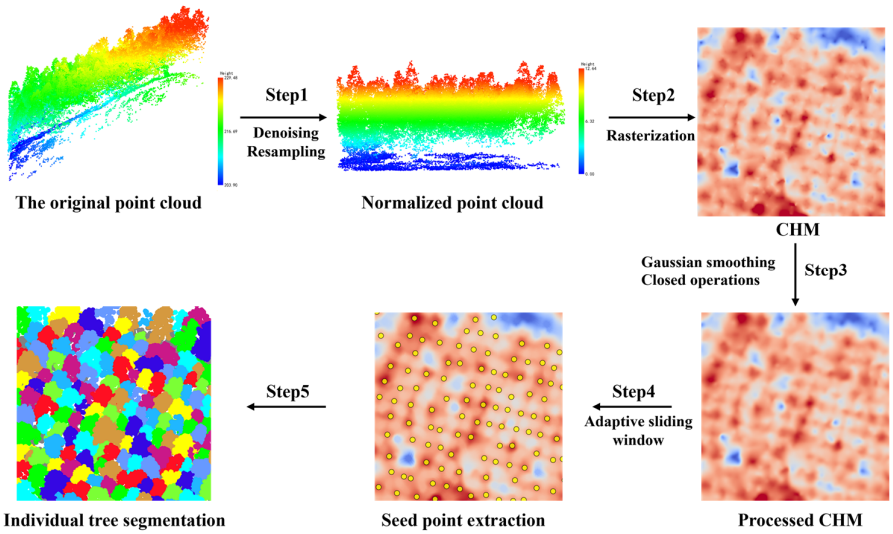

Figure 2. Flowchart of individual tree segmentation.

③ The local maximum method of variable windows is used to detect the vertices of CHM after processing. During the detection process, the detection window scale is automatically selected by setting a canopy height threshold to improve the accuracy of tree vertex extraction. The height information and position information of the vertices of the detection tree are saved as tree heights extracted by the UAV and seed points for single-tree segmentation.

④ Using the seed points extracted as cluster centers, the neighborhood points are aggregated iteratively in the 3D point cloud space by region-growing algorithm to define the canopy boundary of individual trees, and the accurate segmentation of individual trees with complex forest structures is realized by combining the results of Euclidean clustering optimization segmentation.

(2) Crown width extraction based on Alpha-shape algorithm

This study used the Alpha-shape algorithm to delineate the boundaries of individual tree point clouds for crown width extraction. Its basic principle is as follows: for any planar point cloud shape, when a circle with radius r rolls around it, if the radius increases to a certain degree, the rolling trajectory will form the boundary of the point cloud [35]. The Alpha-shape algorithm can construct projections that better match the actual tree crown shape, making the extracted boundaries truly reflect the growth condition of the tree crown (Figure 3).

(3) Construction of single-tree DBH model

The results of crown width extraction based on the Alph-shape algorithm and point cloud feature variables of each tree in the sample plot are calculated to retrieve the DBH of a single tree of Chinese fir, which includes height features, density features, and intensity features. Specific indicators are shown in Table 2.

Table 2. List of variables extracted from UAV-LiDAR point clouds.

Class	Variable	Description
Height variable	H_xth	Height percentile
	H_mean, H_max, H_min, H_median	Mean, maximum, minimum, and median
	H_std, H_cv, H_ske, H_kur, H_cur, H_var	Standard deviation, coefficient of variation, skewness, kurtosis, cubic mean, and variance

Table 2. *Cont.*

Class	Variable	Description
Density variable	D0, D1, D2, D3, D4, D5, D6, D7, D8, D9	The density of the point cloud in each of the ten horizontal layers uniformly divided from low to high
Intensity variable	I_xth	Intensity percentile
	I_mean, I_max, I_min, I_median	Mean, maximum, minimum, and median
	I_std, I_cv, I_ske, I_kur, I_var	Standard deviation, coefficient of variation, skewness, kurtosis, and variance

Note: The variable x represents the percentile values: 1, 5, 10, 20, 25, 30, 40, 50, 60, 70, 75, 80, 90, 95, and 99. Subscripts in feature variables (e.g., mean, max, min, and median) denote the corresponding statistical operations performed on the data.

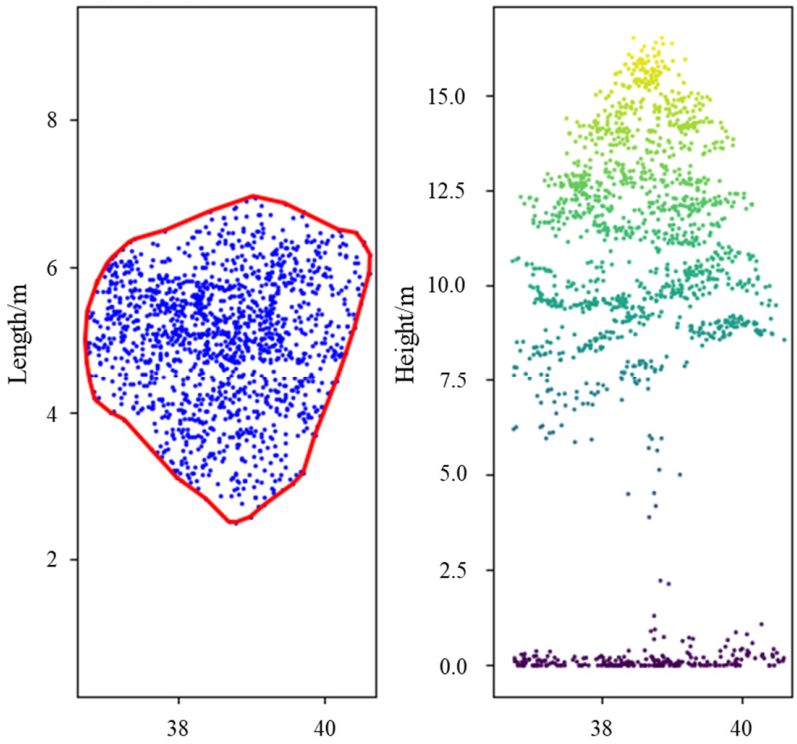

Figure 3. Crown boundary delineation using Alpha-shape algorithm.

Pearson correlation analysis was used to calculate the correlation coefficient between point cloud characteristic variables and measured DBH of individual trees. The closer $|r|$ is to 1, the more significant the correlation between variables and DBH. Then the DBH inversion model of Chinese fir single tree was constructed, with characteristic variables as independent variables and DBH as dependent variables, in which the ratio of training set, test set, and validation set was 7:2:1. The models adopted were as follows: ① BP neural network regression model; ② random forest regression model; and ③ XGBoost regression model.

(4) Accuracy validation

① Single-tree segmentation accuracy.

Based on CHM and cloud data of sample sites, verification data of individual tree positions are obtained by manual interpretation and visual interpretation, and then the accuracy of individual tree segmentation is evaluated by recall rate R, accuracy rate P, and harmonic value F considering R and P, where the maximum value of F is 1 and the minimum value is 0. The results of segmentation can be roughly divided into three cases (Figure 4):

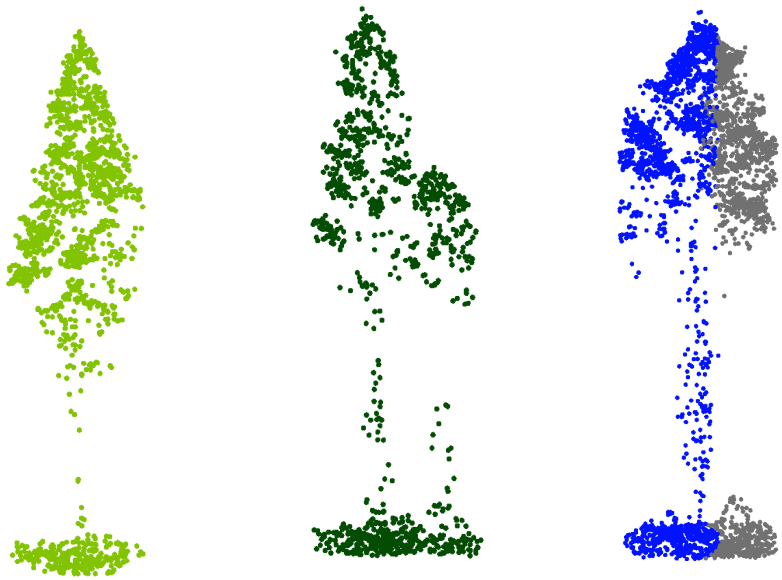

(**a**) (**b**) (**c**)

Figure 4. Schematic diagram of the three results of single-tree segmentation. (**a**) Correct segmentation, (**b**) under-segmentation, and (**c**) over-segmentation.

Correct segmentation P_t The number of Chinese firs correctly partitioned in the sample plot;

Under-segmentation (N_f): The number of Chinese fir trees that are not segmented due to being mistaken by the algorithm as belonging to other Chinese fir trees;

Over-segmentation (P_f): The number of Chinese fir trees that belong to one tree but are mistakenly divided into multiple trees by the algorithm, as shown in the figure. Therefore, R, P, and F are calculated as follows:

$$R = \frac{P_t}{P_t + N_f} \tag{1}$$

$$P = \frac{P_t}{P_t + P_f} \tag{2}$$

$$F = \frac{2P \times R}{P + R} \tag{3}$$

② Accuracy validation of parameter extraction

Accuracy tests for tree height, crown breadth, and DBH models were evaluated using coefficient of determination R^2, root mean square error (RMSE), and mean absolute error (MAE).

2.3.2. Stand Spatial Structure Evaluation Indicators

Weighted Voronoi method was used to extract spatial structure parameters of various sites [36,37]. Based on the tree position information after single-tree segmentation, the weighted Voronoi was constructed by combining the tree height, crown width, and DBH data extracted by UAV, and the spatial structure unit of the stand was determined. Stand spatial structure unit is the smallest unit for calculating spatial structure parameters, which consists of a central tree and several competitive trees. By calculating the angle and distance between the central tree and the competitive trees, the spatial structure parameters of stands can be extracted based on UAV, according to the correlation formula.

We identified six evaluation indicators for assessing stand spatial structure based on resource utilization, growth environment, and growth quality perspectives. The resource

utilization degree, as a first-level index, comprises uniform angle (W) and forest layer index (S). The uniform angle [38] characterizes the horizontal spatial distribution of forest trees, indicating the utilization of horizontal spatial resources by forests. The forest layer index [39] pertains to the vertical stratification of the forest, with a higher complexity of stratification indicating a greater utilization of vertical space resources by the forest. The first-level index for growth environment includes openness (K) and openness ratio (OP). Openness [40] reflects the size of the growth space available for trees, while the openness ratio [41] indicates the light exposure of the tree canopy. Regarding growth quality, the first-level indicators consist of the size ratio (U) and the angle competition index (UCI). The size ratio [42] illustrates the growth discrepancy between the central tree and its competitors, whereas the angle competition index [43] signifies the intensity of competition between the central tree and its competitors. The parameter calculation method is shown in Table A1.

2.3.3. Evaluation of Model Construction

(1) Single weight empowerment method

In order to construct a scientific and reasonable evaluation system for the spatial structure of Chinese fir plantations, we used the entropy weight method [44], the CRITIC method [45], the independence weight coefficient method [46], and the projection pursuit method [47] to calculate the weights of six evaluation indicators. Before calculating the weight, the evaluation indicators need to be normalized for dimensionless processing.

(2) Calculation of comprehensive weights based on game theory

We perform combinatorial empowerment based on game theory, reconcile conflicts between the 4 objective weighting methods, and look for consistency between them. The game theory combinatorial weighting method can integrate the advantages of various weight calculation methods and can also overcome the limitations of each weight calculation method to obtain more accurate and reasonable index weights. The specific calculation process is shown in [48].

(3) Spatial structure evaluation model based on cloud model

Cloud model is an uncertainty transformation model based on probability theory and fuzzy mathematics [49]. The core of the concept is to characterize the statistical characteristics of concepts by three kinds of cloud digital characteristics: expectation (Ex), entropy (En), and hyper-entropy (He). Expectation reflects the distribution center of cloud droplets and can describe the central value of concepts; entropy represents the dispersion range of cloud droplets and describes the fuzziness and randomness of concepts; and hyper-entropy represents the stability of cloud droplets and measures the uncertainty of entropy.

The cloud generator is the key to cloud map generation, which can be divided into forward cloud generator and reverse cloud generator, according to their working mechanism. The reverse cloud generator performs the conversion from cloud droplets to three digital features, while the forward cloud generator performs the conversion from three digital features to cloud droplets, as shown in Figure 5.

The cloud model theory was used to evaluate the spatial structure of Chinese fir plantations systematically.

① Construct an index evaluation set.

Based on the data extracted by UAV, the average value of 6 spatial structure indexes of 5 age groups was calculated. Combined with the actual situation of sample plots, 15 experts were consulted, and 6 spatial structure indexes of different age groups were evaluated and scored. The effective domain was [0, 100]. Then, we constructed an evaluation standard cloud, which can be used as a benchmark for evaluating the spatial structure of Chinese fir plantations. The quality of spatial structure is divided into five grades: I, II, III, IV, and V.

The scoring interval and comprehensive expression corresponding to each grade are shown in Table 3.

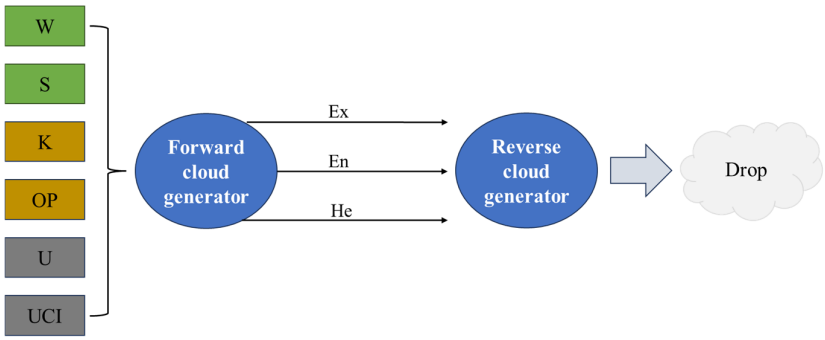

Figure 5. Forward and reverse cloud generator workflow.

Table 3. The evaluation interval of the spatial structure quality of the stand.

Evaluation Level	Evaluation Description	Evaluation Interval
I	Poor quality of space structures	0.0–24.9
II	Suboptimal spatial structure quality	25.0–49.9
III	Moderate spatial structure quality	50.0–74.9
IV	Good spatial structure quality	75.0–89.9
V	Excellent spatial structure quality	90.0–100

The calculation formula for calculating the cloud digital characteristics of the evaluation interval cloud (E_x, E_n, and H_e) is as follows:

$$\begin{cases} E_x = \frac{L_{max}+L_{min}}{2} \\ E_n = \frac{L_{max}+L_{min}}{6} \\ H_e = f \end{cases} \quad (4)$$

where L_{max} is the upper limit of the evaluation interval, L_{min} is the lower limit of the evaluation interval, and f is the fixed value, generally 0.5. The numerical characteristics of the standard cloud are shown in Table 3.

② Calculate the numerical characteristics of the secondary index cloud.

The scoring results of 6 spatial structure parameters in 5 age groups are converted into cloud parameters by the reverse cloud generator, and the steps are as follows:

Calculate the mean

$$\overline{B_j} = \frac{1}{n}\sum_{i=1}^{n} b_{ij} \quad (5)$$

where $\overline{B_j}$ is the average score of the jth indicator, n is the number of experts, and b_{ij} represents the score of the ith expert on the jth indicator.

Calculate variance

$$S_j^2 = \frac{1}{n-1}\sum_{i=1}^{n}\left(b_{ij} - E_{x_j}\right)^2 \quad (6)$$

where S_j^2 is the variance of the jth indicator, and E_{x_j} is the expectation of the jth indicator.

Compute the cloud digital characteristics

$$\begin{cases} E_{x_j} = \overline{B_j} \\ E_{n_j} = \sqrt{\frac{\pi}{2}}\frac{1}{n}\sum_{i=1}^{n}\left|b_{ij} - E_{x_j}\right| \\ H_{e_j} = \sqrt{\left|S_j^2 - {E_{n_j}}^2\right|} \end{cases} \quad (7)$$

where E_{n_j} is the entropy of the jth indicator, and H_{e_j} is the super-entropy of the jth indicator.

③ Calculate the first-level indicators, and comprehensively evaluate the numerical characteristics of the cloud.

The first-level indicators are solved by the floating cloud algorithm, and the index weights calculated by game theory and the numerical characteristics of the second-level indicator cloud are calculated, and the calculation method is as follows:

$$\begin{cases} E_x = \frac{E_{x_1}w_1+E_{x_2}w_2+\cdots+E_{x_j}w_j}{w_1+w_2+\cdots+w_j} \\ E_n = \frac{E_{n_1}{w_1}^2+E_{n_2}{w_2}^2+\cdots+E_{n_j}{w_j}^2}{{w_1}^2+{w_2}^2+\cdots+{w_j}^2} \\ H_e = \frac{H_{e_1}{w_1}^2+H_{e_2}{w_2}^2+\cdots+H_{e_j}{w_j}^2}{{w_1}^2+{w_2}^2+\cdots+{w_j}^2} \end{cases} \quad (8)$$

where w_j is the comprehensive weight of the jth indicator based on game theory, and j is the number of indicators.

The calculation method of the digital features of the comprehensive evaluation cloud is as follows:

$$\begin{cases} E_x = \frac{E_{x_1}E_{n_1}w_1+E_{x_2}E_{n_2}w_2+\cdots+E_{x_j}E_{n_j}w_j}{E_{n_1}w_1+E_{n_2}w_2+\cdots+E_{n_j}w_j} \\ E_n = E_{n_1}w_1 + E_{n_2}w_2 + \cdots + E_{n_j}w_j \\ H_e = \frac{H_{e_1}E_{n_1}w_1+H_{e_2}E_{n_2}w_2+\cdots+H_{e_j}E_{n_j}w_j}{E_{n_1}w_1+E_{n_2}w_2+\cdots+E_{n_j}w_j} \end{cases} \quad (9)$$

Based on the above analysis, we calculate the cloud digital characteristics of three primary indicators and comprehensive evaluation cloud digital characteristics according to the cloud digital characteristics of six secondary indicators. Then, the digital characteristics of the first-level index cloud and the digital characteristics of the comprehensive evaluation cloud are introduced into the forward cloud generator so that the corresponding evaluation cloud map of the spatial structure of the five age groups are obtained, and the positions and shapes of the evaluation cloud map and the standard cloud model map are compared, and the region with the highest coincidence degree of the two is judged as the current grade state.

3. Results

3.1. Accuracy Assessment of UAV Extraction of Single-Tree Parameters

The overall accuracy of each plot is 0.809–0.963, and the average accuracy of the whole is 0.882. Among them, with the increasing age, the recall rate R, the accuracy rate P, and the F values have decreased, but they have basically remained above 0.8. This shows that the accuracy of the single-tree segmentation method used in this study is relatively high, but with the increase in the age of the Chinese fir plantation, the trees are obscuring each other more and more seriously, which leads to errors in the process of seed point extraction, which leads to a decrease in the segmentation accuracy.

From the point of view of tree growth, with the increasing age of Chinese fir plantations, the stand gradually entered the closed state, and the crown shape and spatial structure changed significantly. At the young stage, the distance between trees is relatively large, the canopy structure is relatively simple, and the shielding effect between individual trees is weak. The UAV remote sensing can clearly capture the canopy contour information of individual trees, so the segmentation accuracy is high. With the growth of forest age, the canopy width and height of trees increased, and the canopy overlapping and shielding phenomenon became serious, forming dense canopy coverage. This not only increases the difficulty of single-tree recognition in remote sensing images, but also interferes with the seed point extraction process, which is easy to miss or misextract. In addition, the

vegetation in the middle and lower layers of overripe Chinese fir stands may gradually develop, which further increases the complexity of the canopy structure, resulting in the blurred boundaries and weakened characteristics of individual trees in remote sensing data, thus causing the overall decline in the recall rate, accuracy rate, and F value. Although the accuracy decreases with the increase in forest age, the algorithm is still at a high level because of its strong adaptability, reflecting that the method still has good recognition ability under a complex forest structure (Table 4).

Table 4. Accuracy of single-tree segmentation in each sample plot.

Age Group	Sample Plot NO.	Standard Deviation of Gaussian Kernel	Measured Quantity	Number of Segments	Number of Errors	R	P	F
Young forest	1	0.7	152	140	1	0.914	0.993	0.952
	2	1.2	162	158	4	0.951	0.975	0.963
	3	1.2	193	173	6	0.865	0.965	0.913
Middle-aged forest	4	1.3	83	83	8	0.904	0.904	0.904
	5	2.4	91	91	7	0.923	0.923	0.923
	6	0.7	74	72	3	0.932	0.958	0.945
Near-ripe forest	7	0.3	157	125	11	0.726	0.912	0.809
	8	2.5	149	127	1	0.846	0.992	0.913
	9	0.7	135	130	13	0.867	0.900	0.883
Mature forest	10	2.5	40	38	9	0.800	0.842	0.821
	11	3	62	70	11	0.887	0.786	0.833
	12	1.7	88	90	10	0.875	0.856	0.865
Overripe forest	13	1.8	112	108	15	0.830	0.861	0.845
	14	2.5	44	40	6	0.773	0.850	0.810
	15	1.5	102	98	13	0.833	0.867	0.850

Subsequently, we randomly selected about 10 trees in each sample plot to ensure that there were no less than 30 trees in each age group, with a total of 153 trees, which were used for the accuracy verification of the tree height and crown width extracted by drones. The accuracy of the tree height extraction reaches 0.964 (RMSE = 0.983 m, MAE = 0.626 m) (Figure 6), and most of the residuals between the measured tree height and the estimated tree height are within the range of (−1, 1) (Figure 7). The Alpha-shape algorithm was used to extract the crown amplitude, and the accuracy was 0.862 (RMSE = 0.335 m, MAE = 0.232 m) (Figure 8), and most of the residuals between the measured and estimated values were in the range of (−0.2, 0.2) (Figure 9). On the whole, the accuracy of the tree height and crown width extracted by drones is relatively high.

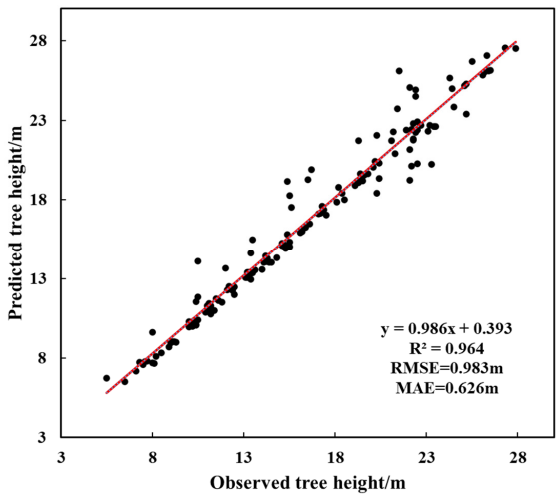

Figure 6. UAV estimation accuracy of tree height.

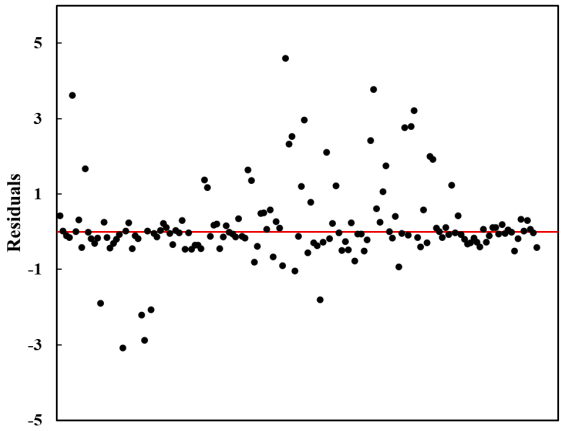

Figure 7. UAV tree height prediction residual.

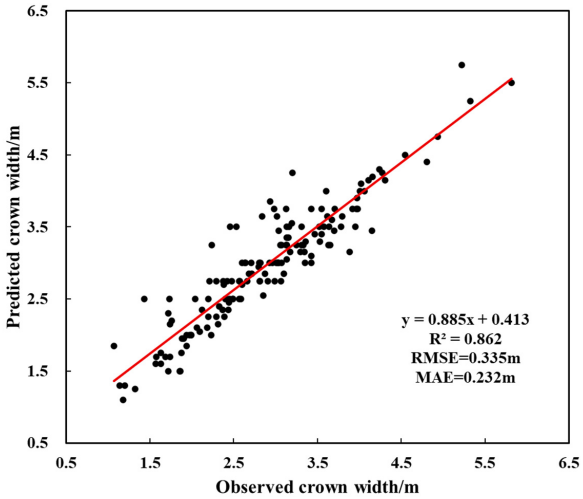

Figure 8. UAV estimation accuracy of crown width.

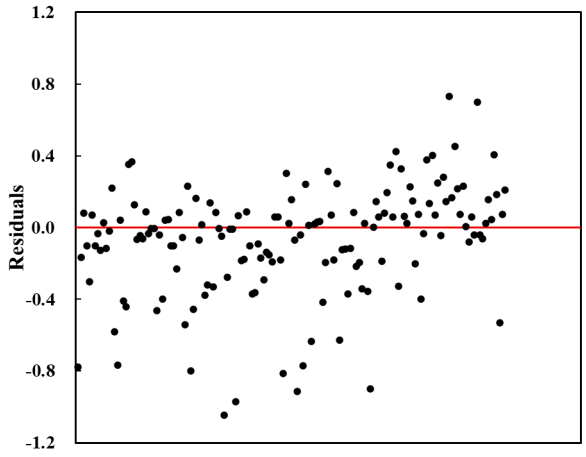

Figure 9. UAV crown width prediction residual.

3.2. Results of Single-Tree DBH Model Construction

Based on the 153 trees used for data verification, a DBH model of a single tree was constructed, and the variable characteristics were screened out by a Pearson correlation test. Among them, there was a positive correlation between the height variable and DBH of Chinese firs, while density characteristics and strength characteristics basically showed a weak negative correlation (Table 5).

Table 5. Variable filter results.

Variable	Correlation	Variable	Correlation	Variable	Correlation	Variable	Correlation	Variable	Correlation
H_cur	0.720 ***	H_1th	0.318 ***	H_50th	0.737 ***	H_99th	0.765 ***	I_ske	0.158 *
H_max	0.769 ***	H_5th	0.572 ***	H_60th	0.745 ***	D0	−0.121 **	I_std	0.272 ***
H_mean	0.703 ***	H_10th	0.633 ***	H_70th	0.747 ***	D1	−0.185 **	I_10th	−0.277 ***
H_median	0.706 ***	H_20th	0.682 ***	H_75th	0.751 ***	D4	−0.22 ***	I_20th	−0.259 ***
H_ske	−0.25 ***	H_25th	0.698 ***	H_80th	0.751 ***	D7	0.169 **	I_30th	−0.161 *
H_std	0.632 ***	H_30th	0.704 ***	H_90th	0.759 ***	I_cv	0.332 ***	I_90th	0.173 **
H_var	0.584 ***	H_40th	0.713 ***	H_95th	0.76 ***	I_max	0.428 ***	I_95th	0.209 **

Note: *p*-values significance levels: * $p < 0.05$, ** $p < 0.01$, *** $p < 0.001$.

The DBH model was constructed by taking the measured DBH as the dependent variable and point cloud characteristics as the independent variable. The results are shown in the table. In the process of model construction, the XGBoost model always has the highest accuracy in both the training set and test set, where the training set is R^2 = 0.982, RMSE = 1.428 cm, and MAE = 0.759 cm, and the test set is R^2 = 0.869, RMSE = 3.788 cm, and MAE = 3.101 cm. The graph reflects the results of the three model validation sets, showing the correlation, standard deviation, and root mean square error between the estimated values and the measured values. When the results are closer to the Observed point, the model performance is better (Figure 10). Therefore, it can be seen that the performance of the XGBoost regression model remains optimal during the model validation process. Therefore, the XGBoost model is used in this paper to realize the inversion of the DBH of Chinese firs (Table 6).

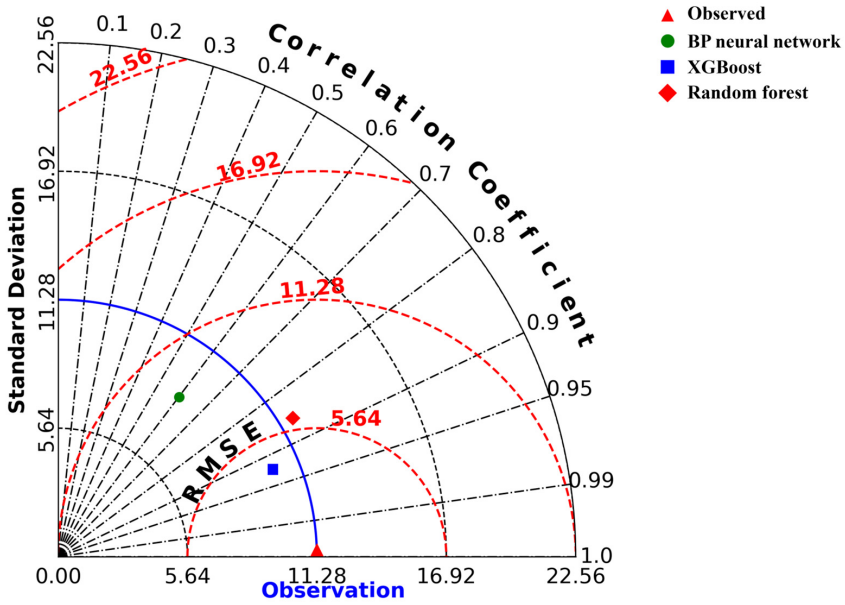

Figure 10. Model validation set—Taylor diagram.

Table 6. Machine learning model performance comparison.

Regression Model	Data Set					
	Training Set			Test Set		
	R^2	RMSE	MAE	R^2	RMSE	MAE
BP neural network	0.744	5.221	3.911	0.556	7.485	5.433
Random forest	0.929	2.866	1.943	0.789	4.681	3.378
XGBoost	0.982	1.428	0.759	0.869	3.788	3.101

3.3. Construction of Spatial Structure Evaluation System of Chinese Fir Plantation

3.3.1. Parameter Extraction Results for Spatial Structure of Stands

Table A2 reflects the age-based change process of spatial structure parameters of Chinese fir plantations. The size ratio increased first and then decreased, with the most obvious growth disadvantage in the middle-aged forest stage (0.529); the angle competition index also increased first and then decreased, and the competition in the middle-aged forest (0.329) was the most intense. The openness and openness ratio continued to decrease, from sufficient space (0.304) and a good light reception (0.901) in young forests to a severe deficiency (0.161) and weakening light reception (0.695) in overripe forests. The uniform angle was optimized from the cluster distribution of young forests (0.754) to the random distribution of overripe forests (0.482). The forest layer index continued to rise, and the vertical structure developed from simple (0.245 in young forests) to more complex (0.509 in overripe forests).

3.3.2. Evaluation Results of Forest Stand Spatial Structure

(1) Combination weighting

After preprocessing the spatial structure parameters of the six stands, the weights were calculated by using the entropy weight method, the CRITIC method, the independence weight coefficient method, and the projection pursuit method, and then the weights were combined based on the game theory. The combined weights of each index are U = 25.08%, UCI = 9.94%, K = 19.88%, OP = 11.44%, W = 13.05%, and S = 20.61%, and the weight of the size ratio, forest layer index, and openness is relatively large (Figure 11).

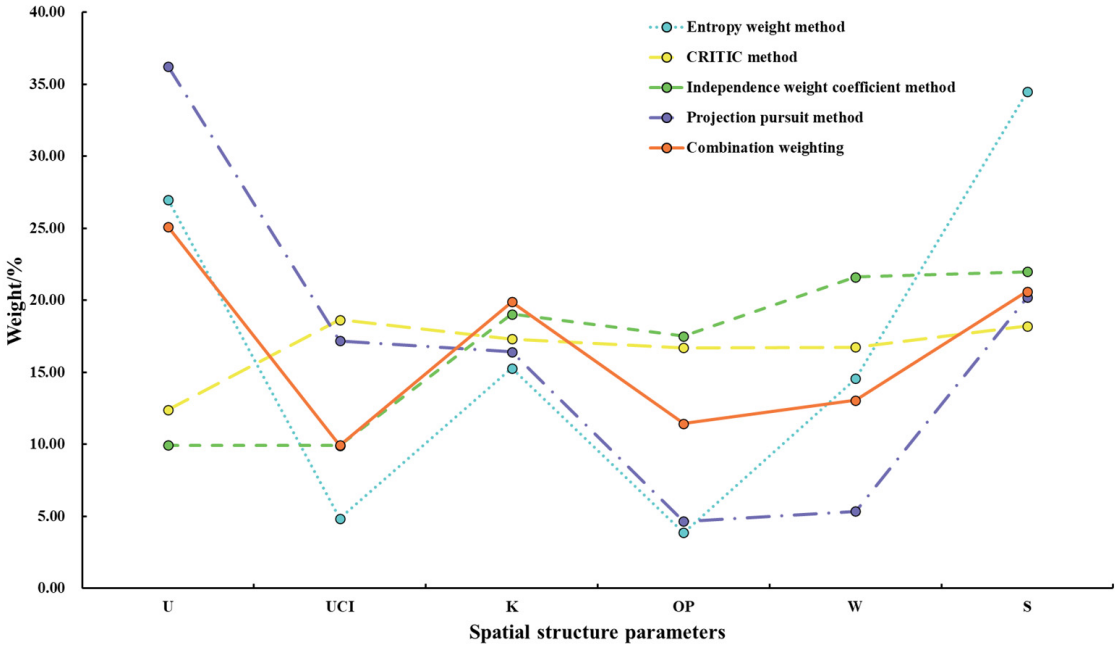

Figure 11. Comparison of results of different weighting methods.

(2) Evaluation based on cloud models

The cloud model was used to evaluate the rationality of the spatial structure of the Chinese fir plantation. Based on the extraction results of the structural parameters of different age groups and the actual situation in the forest, experts scored them. According to the combination formula of the reverse cloud generator, the cloud numerical characteristics of each secondary index are calculated, and the specific results are shown in Table 7.

Table 7. Secondary indicator cloud digital characteristics.

Age Group	Cloud Digital Characteristics	Spatial Structure Parameters					
		U	UCI	K	OP	W	S
Young forest	Ex	56.933	60.000	67.067	85.867	42.267	36.000
	En	4.601	3.509	4.768	3.041	5.036	4.011
	He	0.496	1.083	1.292	0.642	1.928	1.171
Middle-aged forest	Ex	35.533	43.200	43.933	85.400	53.200	40.200
	En	3.554	8.890	5.771	3.476	7.921	8.121
	He	1.032	3.360	1.632	1.351	2.420	1.488
Near-ripe forest	Ex	45.800	46.267	43.800	85.000	68.133	56.867
	En	8.924	7.041	5.281	4.345	5.715	4.835
	He	3.932	1.168	1.648	1.143	1.119	1.919
Mature forest	Ex	63.400	64.200	33.800	74.933	78.133	76.000
	En	4.378	5.615	3.743	3.097	3.565	4.345
	He	1.395	0.888	1.642	0.817	1.554	1.565
Overripe forest	Ex	76.400	88.600	29.800	67.933	93.133	83.000
	En	4.378	4.946	3.743	3.097	3.565	4.345
	He	1.395	0.799	1.642	0.817	1.554	1.565

According to the floating cloud computing method, based on the combination weights of the secondary indicators obtained by the game theory method and their three cloud digital characteristics, the cloud digital characteristics of the primary indicators of different age groups of Chinese firs and the digital characteristics of the comprehensive evaluation cloud are calculated by Equations (8) and (9). The results are shown in the table. According to the first-level indicators' characteristics and comprehensive cloud characteristics, the evaluation cloud map is drawn by a forward cloud generator (Table 8).

Table 8. Cloud digital characteristics of first-level indicators and comprehensive evaluation.

Age Group	First-Level Indicators	Cloud Digital Characteristics (Ex, En, and He)
Young forest	growth quality	(57.871, 4.423, 0.591)
	growth environment	(74.220, 4.295, 1.114)
	resource utilization	(38.645, 4.367, 1.434)
	comprehensive evaluation cloud	(55.925, 4.699, 1.087)
Middle-aged forest	growth quality	(37.878, 4.422, 1.411)
	growth environment	(59.709, 5.143, 1.555)
	resource utilization	(45.686, 8.051, 1.812)
	comprehensive evaluation cloud	(46.245, 6.616, 1.907)
Near-ripe forest	growth quality	(45.943, 8.618, 3.482)
	growth environment	(59.475, 5.025, 1.510)
	resource utilization	(61.621, 5.141, 1.641)
	comprehensive evaluation cloud	(53.271, 6.850, 2.325)
Mature forest	growth quality	(63.645, 4.579, 1.313)
	growth environment	(49.449, 3.566, 1.416)
	resource utilization	(76.900, 4.074, 1.561)
	comprehensive evaluation cloud	(63.462, 4.521, 1.364)
Overripe forest	growth quality	(80.132, 4.470, 1.298)
	growth environment	(44.308, 3.566, 1.416)
	resource utilization	(87.276, 4.074, 1.561)
	comprehensive evaluation cloud	(71.989, 4.441, 1.361)

① Young forest.

According to the results of the cloud model evaluation (Figure 12), the overall spatial structure of the young forest of Chinese firs was at level III (general level), indicating that the current structural status of the stand was basically reasonable, but there was still some room for optimization. Specifically, the growth environment was ideal (level IV), indicating that the two indexes of openness and the openness ratio performed well, and the stand had sufficient sunlight exposure and growth space, which was conducive to the initial growth of trees. The growth degree was at a moderate level (level III), indicating that the individual differentiation of forest trees and resource competition was within the normal range, but there was room for optimization, and the competitive pressure might need to be reduced by adjusting the planting density. The degree of resource utilization is relatively poor (level II), which reflects that the horizontal distribution and vertical stratification of stands are not reasonable enough, which is manifested in the insufficient randomness of the forest distribution and single level, resulting in the low utilization rates of light, heat, nutrients, and other resources.

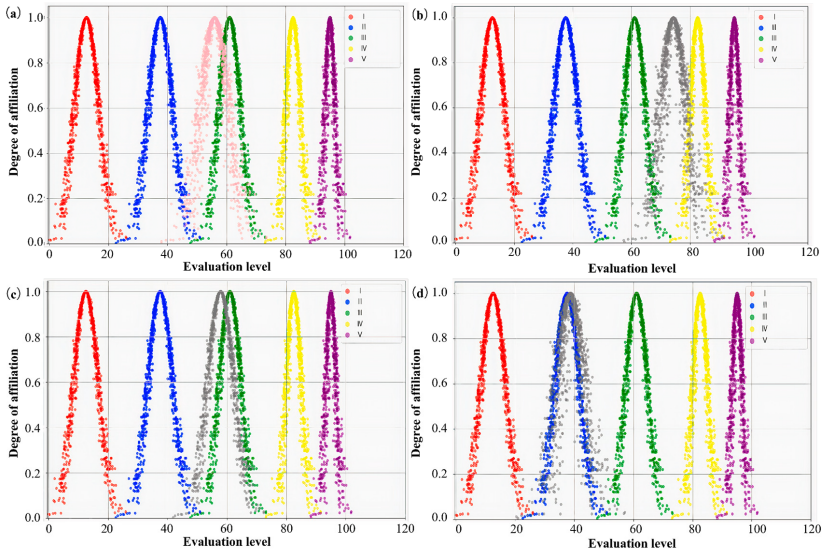

Figure 12. Young forest evaluation cloud map. (**a**) Comprehensive evaluation cloud; (**b**) growth environment evaluation cloud; (**c**) growth quality evaluation cloud; and (**d**) resource utilization evaluation cloud. The pink cloud map represents the comprehensive evaluation results, while the gray cloud map represents the evaluation results of each primary indicator.

② Middle-aged forest.

The spatial structure of the middle-aged Chinese fir stand was in level II (poor level), which indicated that there were obvious defects in the structure of the stand, and reasonable management measures should be taken to optimize and adjust it (Figure 13). Specifically, the growth environment (level III) is at a general level, indicating that the stand openness and open ratio basically meet the growth needs of trees, but the light conditions and spatial distributions have been limited to some extent, which may affect the sustainable and healthy growth of trees. The poor performance of growth quality (level II) reflected that the size differentiation of individual trees was quite different, the competition pressure was greater, and some weak trees might have been significantly inhibited, resulting in the unbalanced growth of the whole stand. The resource utilization degree (level II) was also poor, indicating that the horizontal distribution and vertical structure of the stand were unreasonable, the spatial allocation efficiency was low, and the resources such as light, water, and nutrients could not be fully utilized.

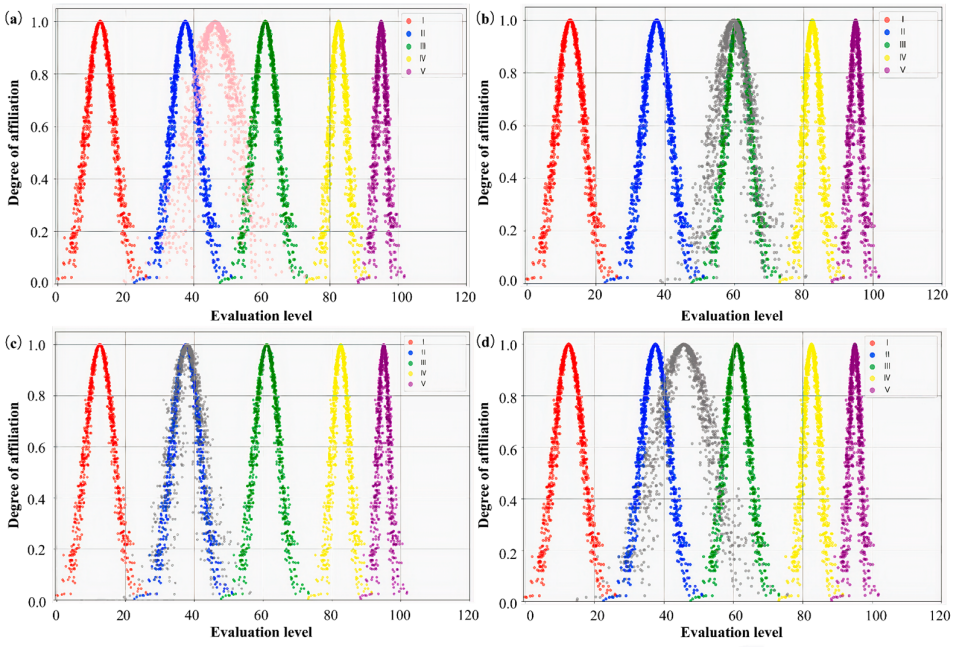

Figure 13. Middle-aged forest evaluation cloud map. (**a**) Comprehensive evaluation cloud; (**b**) growth environment evaluation cloud; (**c**) growth quality evaluation cloud; and (**d**) resource utilization evaluation cloud. The pink cloud map represents the comprehensive evaluation results, while the gray cloud map represents the evaluation results of each primary indicator.

③ Near-ripe forest.

According to the evaluation results, the spatial structure of the stand was between II and III, which indicated that, although there were some problems in the stand structure, there was a foundation for it to develop to a better state (Figure 14). From the specific indicators, the growth environment (level III) is in the middle level, indicating that the stand openness and open ratio are basically reasonable, which can maintain the normal growth demand of trees, but there is still room for improvement. The growth quality of trees was slightly worse (level II), which reflected that there was an obvious size differentiation among individual trees, and the competition pressure was too large. Some individuals with weak growth might face the problem of insufficient resource acquisition, but compared with middle-aged forests, it was improved. The resource utilization degree (level III) reached the general level, indicating that the horizontal distribution and vertical structure of the stand gradually tended to be reasonable, and the spatial resource allocation efficiency was still acceptable, but it had not reached the optimal state.

④ Mature forest.

The spatial structure of the mature Chinese fir forest was restored to level III (general level) and a little better, which indicated that the stand had reached a relatively stable structural state after long-term natural succession and structural adjustment, but there was still some room for optimization (Figure 15). The growth environment was relatively weak at level II, reflecting that the open degree and open ratio decreased with the maturity of the stand, and the light condition in the stand might be limited, which accorded with the natural development characteristics of mature forest. The growth quality was in level III, indicating that after long-term competition, the size differentiation among individual trees tended to be stable, and the competitive pressure was relieved, but some individuals were still in a suppressed state. The degree of resource utilization was level III, tending to level IV, indicating that the angular distribution and forest layer index of the mature forest had reached a better level, the spatial allocation and vertical structure were reasonable, and the resource utilization efficiency was high.

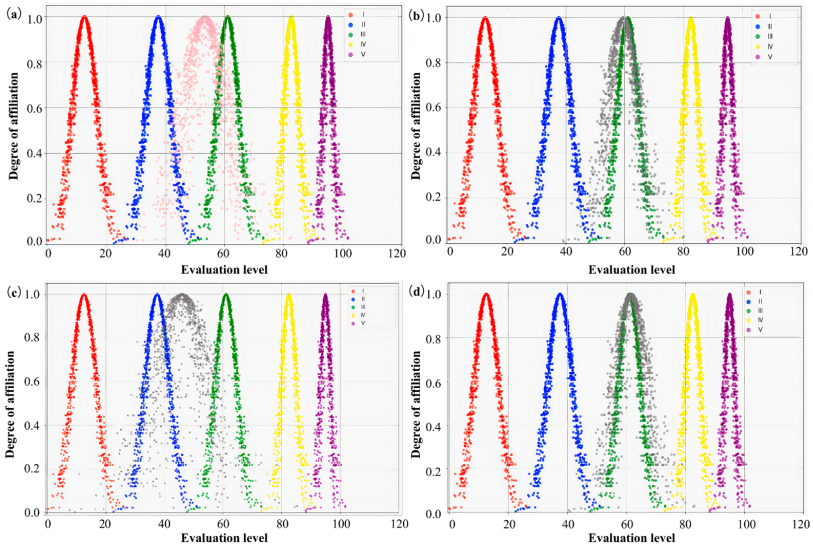

Figure 14. Near-ripe forest evaluation cloud map. (**a**) Comprehensive evaluation cloud; (**b**) growth environment evaluation cloud; (**c**) growth quality evaluation cloud; and (**d**) resource utilization evaluation cloud. The pink cloud map represents the comprehensive evaluation results, while the gray cloud map represents the evaluation results of each primary indicator.

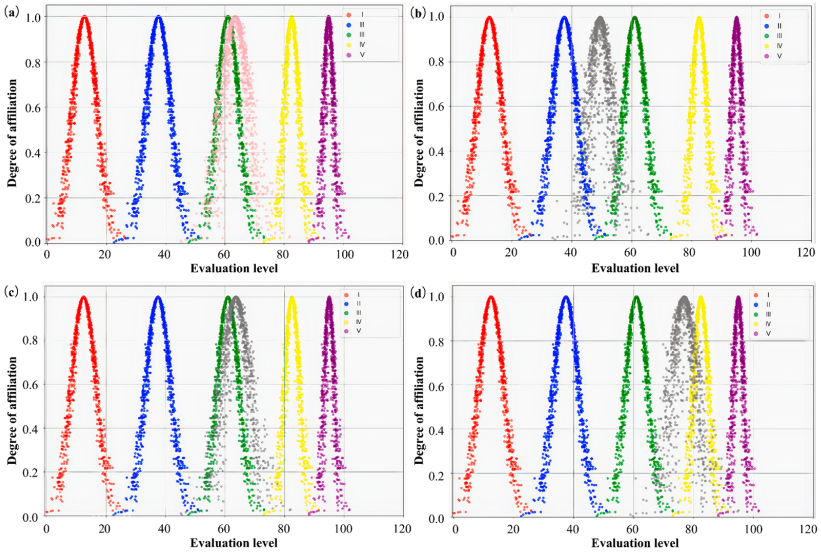

Figure 15. Mature forest evaluation cloud map. (**a**) Comprehensive evaluation cloud; (**b**) growth environment evaluation cloud; (**c**) growth quality evaluation cloud; and (**d**) resource utilization evaluation cloud. The pink cloud map represents the comprehensive evaluation results, while the gray cloud map represents the evaluation results of each primary indicator.

⑤ Overripe forest.

The spatial structure of the overripe Chinese fir forest was in transition from III to IV, showing obvious characteristics of "structure optimization but environmental degradation" (Figure 16). Concretely speaking, the significant decrease in the growth environment index (level II) indicates that the open degree and open ratio obviously decrease, and the light condition deteriorates with the stand entering the overripe stage, which reflects the typical characteristics of natural senescence of an overripe forest. However, the growth quality (level IV) reached a good level, indicating that after long-term natural selection, a stable growth relationship between individual trees was formed, the intraspecific competition pressure had been significantly reduced, and the dominant trees and the suppressed trees

formed a relatively balanced coexistence state. The resource utilization degree (level IV) also performed well, indicating that the angular scale distribution of the overripe forest tended to be reasonable through long-term succession, and the forest layer index reached a better level, forming an efficient spatial resource allocation pattern.

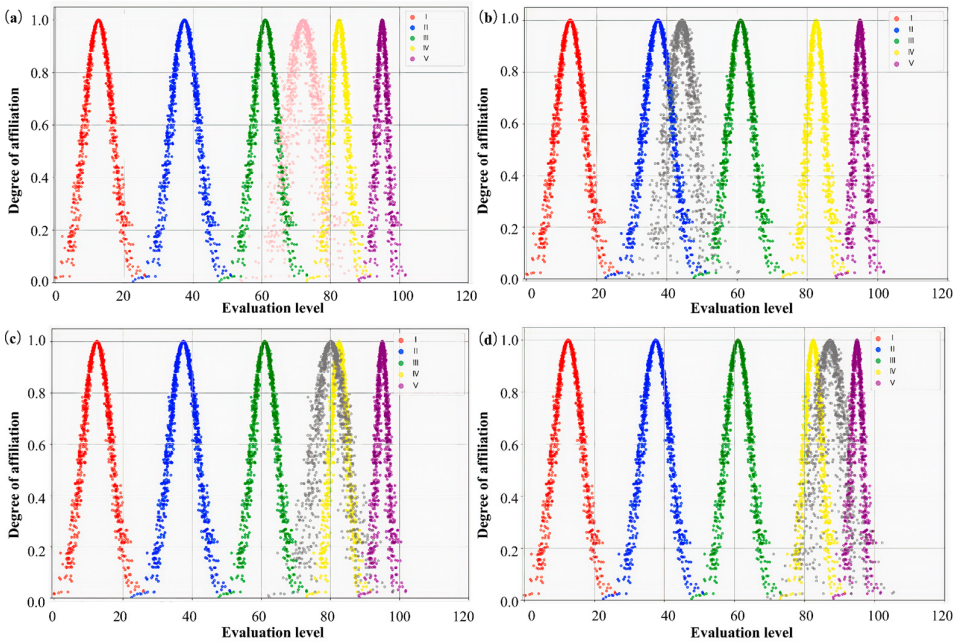

Figure 16. Overripe forest evaluation cloud map. (**a**) Comprehensive evaluation cloud; (**b**) growth environment evaluation cloud; (**c**) growth quality evaluation cloud; and (**d**) resource utilization evaluation cloud. The pink cloud map represents the comprehensive evaluation results, while the gray cloud map represents the evaluation results of each primary indicator.

The spatial structure characteristics of Chinese fir plantations at different development stages showed obvious dynamic changes. According to the evaluation results, the growth environment indexes showed a downward trend with the growth of the forest age (level IV of the young forest to level II of the overripe forest), reflecting the deterioration of light conditions caused by the increase in stand canopy closure; the growth quality showed a "V"-shaped change (level III of the young forest to level II of the middle-aged forest to level IV of the overripe forest), indicating that the competition in the middle-aged stage was the most intense, while the overripe stage tended to be stable; and the resource utilization degree continued to improve (level II of the young forest to level IV of the overripe forest), indicating that natural selection promoted the continuous optimization of spatial allocation. The comprehensive evaluation results showed that the structure quality increased gradually after the "middle age valley", which revealed that there was an obvious ecological process of "competition-adaptation-optimization" in the developmental process of a Chinese fir plantation (Table 9).

Table 9. Evaluation results of stand spatial structure of Chinese fir plantation.

Age Group	Growth Environment	Growth Quality	Resource Utilization	Comprehensive Evaluation
Young forest	IV	III	II	III
Middle-aged forest	III	II	II	II
Near-ripe forest	III	II	III	III
Mature forest	II	III	IV	III
Overripe forest	II	IV	IV	IV

4. Discussion

4.1. Extraction of Stand Spatial Structure Parameters

In this study, we extracted the parameters of individual trees based on the UAV point cloud data, and constructed a weighted Voronoi diagram based on the tree height, crown width, DBH, and position information of Chinese firs to extract six spatial structure parameters of Chinese fir plantations, which effectively proved the feasibility of UAV point cloud data in the rapid extraction of spatial structure parameters, but there are still certain limitations. From the perspective of factor selection constructed by weighted Voronoi plots, this study is mainly based on the tree height, crown width, and DBH of individual trees as the weight factors. This integrates the basic information of the forest growth status and competitiveness to a certain extent, but there is still the problem of incomplete information dimensions. First of all, DBH, as a representative variable of the status index, usually needs to be inverted with the help of empirical models or ground plot support in remote sensing point clouds, which is greatly affected by measurement errors and model accuracy [50,51]. In addition, the spatial expression of competition is also restricted by other key factors, such as canopy morphology, leaf area index, trunk straightness, etc. [52–54], that are not included in the weight calculation, and these factors may also have a certain impact on the division of structural units. Therefore, subsequent studies can try to introduce more ecologically significant parameters based on light acquisition potential, canopy overlap index, canopy permeability, etc., to improve the expression ability of weighted Voronoi graphs on individual spatial advantages, so that they are closer to the state of forests in actual resource competition.

In the process of extracting spatial structure parameters, we use the point cloud data after elevation normalization to eliminate the influence of terrain relief [55]. The advantage of this processing method is that it can eliminate the errors caused by terrain changes in the extraction of individual tree segmentation, tree height, crown width, etc., and can also effectively reduce the time cost of large-scale point cloud data processing [56]. However, from the perspective of ecological processes, the existence of microtopography in woodland is often an important factor affecting the spatial competition pattern, resource acquisition efficiency, and structural evolution trend of forest trees. Small-scale topographic changes such as slope, slope orientation, depressions, and gullies will directly affect the availability of light, water, and soil nutrients of trees, thereby shaping the growth advantages and competitive relationships of forests [56–59]. Therefore, although elevation normalization can improve the accuracy of parameter extraction, it may also mask the terrain-driven ecological mechanism to a certain extent, resulting in a decrease in the interpretation of spatial structure parameters.

4.2. Construction of Stand Spatial Structure Evaluation System

In this study, an evaluation system for the spatial structure of Chinese fir plantations was constructed based on the combined weight of game theory and cloud models, and the comprehensive evaluation was carried out from three dimensions: resource utilization, growth environment, and growth quality. In the weight determination, four objective weighting methods, namely, the entropy weighting method, CRITIC method, independence weight coefficient method, and projection tracing method, are integrated to effectively overcome the limitations of a single method and improve the rationality and accuracy of weight distribution through game theory optimization and integration [60–64]. In addition, in order to realize the uncertain mapping between quantitative evaluation indicators and qualitative evaluation levels, the cloud model is applied to the spatial structure evaluation of stands. Compared with traditional membership functions or fuzzy comprehensive evaluation methods, cloud models can not only effectively express the gradient relation-

ship between evaluation-level boundaries and avoid artificial fractures in the process of classification but also reflect the uncertain characteristics of samples through cloud droplet distribution and improve the reliability of evaluation results [65–67]. In the evaluation of stand spatial structures, structural indicators are often affected by factors such as measurement accuracy and ecological heterogeneity, and the introduction of cloud models provides mathematical support for such a comprehensive evaluation with ambiguous boundaries and uncertainties. Therefore, the evaluation method based on combined weights and cloud models has certain feasibility in the evaluation of the stand spatial structure.

According to the evaluation results of this study, the dynamic law of stand structure evolution with age in Chinese fir plantations in hilly areas of southern China was revealed. The growth environment index showed a decreasing trend with forest age, which was mainly due to the increasing canopy density of stands with age. The openness and openness ratio of young forests are high, which provide sufficient light conditions and spatial resources, which are conducive to the balanced growth of trees [68]. In the over-mature forest stage, the openness decreased to 0.161, indicating that the canopy was severely closed and the understory habitat deteriorated, which was in line with the natural law of gradual encryption of the canopy structure during forest succession [69]. Wu et al. [70] analyzed the spatial structure characteristics of fir forests of different age groups and found that the average openness of young forests was 0.7157, 0.3368 for middle-aged forests, and 0.2495 for near-mature forests, respectively, indicating that the increase in forest age would lead to the gradual encryption of the canopy. The results show that, although the numerical level varies due to the difference in site conditions and management measures, the gradual closure of the canopy layer is a common law in the process of stand succession. The growth quality index showed a change in the process of first decreasing and then rising, reflecting the phased fluctuation of stand competition. The size ratio and angle competition index of middle-aged forests reached the highest values, respectively, indicating that this stage was the period of the most intense intraspecific competition. At this stage of development, individual trees have entered a period of rapid growth, and the rapid expansion of tree height and crown width has led to a significant increase in the space demand of the aboveground part; the root system has also reached a vigorous stage, and the absorption capacity of underground nutrients and water has been greatly improved. With the continuous improvement of stand canopy density, canopy branches and leaves interlaced to form a dense shade environment, light resources became a limiting factor, and the staggered distribution of underground roots also intensified the competition for nutrients and water. At this time, there was fierce competition among individual trees for limited niche space and resources, which was manifested in morphological adaptation phenomena such as canopy extrusion and partial crown growth. This competitive pressure pushes stands to enter a critical stage of natural thinning, and inferior trees are gradually eliminated due to insufficient resource acquisition, forming a typical self-thinning process [71,72]. As the stands entered the near-maturity and maturity stages, the inferior trees were phased out under the conditions of natural sparseness and continuous competition, the growth dominant individuals obtained more resource space, and the structure tended to be optimized; the size ratio dropped to 0.470 at the overripe forest stage, and the overall growth status improved, indicating that the increase in forest age had a positive impact on optimizing the stand structure [73]. In this study, the change process of growth quality indexes decreased first and then increased, which was consistent with the ecological thinning theory proposed by Reynolds and Ford [74], especially the phenomenon of the surge in competition in the middle-aged forest stage, confirming the “competitive asymmetry” mechanism of the ecological thinning theory. This theory pointed out that when the canopy density of the stand reached the critical point, the dominant trees formed shade stress through vertical

layering, resulting in the decline of the photosynthetic capacity of the inferior trees rather than simple horizontal spatial competition. In addition, the fierce competition in middle-aged forests actually triggers the self-sparseness mechanism of the stand and then shows the phenomenon that the dominant trees play a competitive role first, and the pressed trees die later. Therefore, in future operations, we can break the asymmetric pattern of light resource competition through timely thinning interventions; that is, remove some dominant trees in the middle-aged forest stage, reduce the shade intensity of the canopy, delay the decline process of compacted trees, and improve the overall stability of the stand. The resource utilization index showed a continuous increase with forest age, reflecting the self-optimization ability of the spatial structure. The structure of young forests is simple, the vertical stratification is not obvious, the horizontal pattern is biased towards clusters, and the resource utilization efficiency is limited. With the increase in forest age, forest trees gradually formed vertically complex and horizontally random structural characteristics through niche differentiation and morphological plasticity adjustments [75], and the forest layer index and uniform angle increased to 0.509 and 0.482, respectively, which significantly enhanced the utilization capacity of spatial resources. Based on the above law, the continuous deterioration of the growth environment is the inevitable result of the development of Chinese fir stands, and the phased fluctuation of growth quality reflects the dynamic change in competitive relations, while the gradual improvement of resource utilization reflects the self-optimization ability of stand structures. The stand spatial structure evaluation system constructed in this study provides a scientific quantitative tool and decision-making basis for the precise management and sustainable management of Chinese fir plantations.

5. Conclusions

In this study, the point cloud data obtained by UAV with lidar photogrammetry was used to extract the stand parameters of Chinese fir plantations, and a stand spatial structure evaluation system was constructed based on game theory and cloud model theory. The results showed that the system could effectively reveal the evolution of the stand structure with its developmental stage: young forests had an excellent environment but insufficient resource utilization; competition in middle-aged forests is fierce, and the growth status is declining; near-mature to mature forests improve resource utilization through natural selection; and overripe forests have a weakened environmental bearing capacity but stable structure. The study clarified the key management nodes of thinning and competition in middle-aged forests, structural adjustment in near-mature forests, and structural protection in overripe forests, which provided the theoretical basis and practical guidance for the precise management of Chinese fir plantations.

Author Contributions: Conceptualization, J.L.; methodology, J.L. and B.J.; software, B.J. and X.H.; validation, J.L. and B.J.; formal analysis, J.L. and B.J.; investigation, X.H. and B.J.; resources, X.H. and J.L.; data curation, X.H. and B.J.; writing—original draft preparation, J.L.; writing—review and editing, X.H., G.D. and J.D.; visualization, J.L., X.H. and B.J.; supervision, G.D. and J.D.; project administration, J.D.; funding acquisition, J.D. and G.D. All authors have read and agreed to the published version of the manuscript.

Funding: This research was supported by the Innovation Fund of Fujian Agriculture and Forestry University, grant number KFB23175A.

Data Availability Statement: The data that support the findings of this study are available from the author upon reasonable request.

Conflicts of Interest: The authors declare no conflicts of interest.

Appendix A

Table A1. Results of extracting spatial structure parameters of stands in each sample plot.

Sample Plot NO.	Spatial Structure Parameters											
	U	Mean	UCI	Mean	K	Mean	OP	Mean	W	Mean	S	Mean
1	0.494 ± 0.029	0.475 ± 0.179 B	0.246 ± 0.019	0.253 ± 0.011 C	0.313 ± 0.011	0.304 ± 0.004 A	0.914 ± 0.014	0.901 ± 0.008 A	0.758 ± 0.017	0.754 ± 0.009 A	0.205 ± 0.015	0.245 ± 0.012 C
2	0.480 ± 0.307		0.260 ± 0.018		0.304 ± 0.004		0.871 ± 0.015		0.761 ± 0.016		0.230 ± 0.013	
3	0.455 ± 0.324		0.254 ± 0.194		0.296 ± 0.003		0.918 ± 0.013		0.744 ± 0.015		0.302 ± 0.027	
4	0.550 ± 0.049	0.529 ± 0.027 A	0.329 ± 0.027	0.329 ± 0.016 A	0.269 ± 0.007	0.253 ± 0.004 B	0.895 ± 0.017	0.864 ± 0.012 A	0.721 ± 0.022	0.709 ± 0.012 A	0.376 ± 0.044	0.282 ± 0.022 C
5	0.514 ± 0.045		0.324 ± 0.024		0.236 ± 0.005		0.874 ± 0.016		0.716 ± 0.019		0.215 ± 0.028	
6	0.527 ± 0.048		0.335 ± 0.031		0.259 ± 0.006		0.823 ± 0.028		0.688 ± 0.023		0.254 ± 0.038	
7	0.524 ± 0.036	0.506 ± 0.021 A	0.320 ± 0.024	0.312 ± 0.014 A	0.272 ± 0.009	0.237 ± 0.005 B	0.771 ± 0.022	0.775 ± 0.014 B	0.664 ± 0.016	0.644 ± 0.013 B	0.279 ± 0.018	0.351 ± 0.016 B
8	0.503 ± 0.038		0.306 ± 0.025		0.249 ± 0.007		0.781 ± 0.026		0.631 ± 0.019		0.34 ± 0.003	
9	0.488 ± 0.402		0.309 ± 0.027		0.184 ± 0.003		0.773 ± 0.029		0.633 ± 0.017		0.435 ± 0.004	
10	0.512 ± 0.074	0.494 ± 0.029 B	0.294 ± 0.051	0.285 ± 0.019 B	0.202 ± 0.009	0.183 ± 0.004 C	0.659 ± 0.053	0.742 ± 0.019 B	0.502 ± 0.036	0.571 ± 0.015 B	0.485 ± 0.045	0.472 ± 0.020 A
11	0.475 ± 0.049		0.281 ± 0.033		0.182 ± 0.004		0.720 ± 0.033		0.596 ± 0.026		0.478 ± 0.027	
12	0.503 ± 0.041		0.285 ± 0.026		0.176 ± 0.005		0.796 ± 0.021		0.579 ± 0.021		0.449 ± 0.035	
13	0.464 ± 0.034	0.470 ± 0.023 B	0.234 ± 0.019	0.246 ± 0.014 C	0.173 ± 0.004	0.161 ± 0.003 C	0.739 ± 0.013	0.695 ± 0.012 C	0.477 ± 0.019	0.482 ± 0.013 C	0.497 ± 0.021	0.509 ± 0.022 A
14	0.481 ± 0.067		0.278 ± 0.046		0.196 ± 0.008		0.523 ± 0.039		0.484 ± 0.028		0.541 ± 0.051	
15	0.466 ± 0.035		0.247 ± 0.021		0.135 ± 0.004		0.711 ± 0.018		0.487 ± 0.019		0.473 ± 0.023	

Note: Uppercase letters in the table indicate a very significant difference, $p < 0.01$.

Table A2. Calculation method of stand spatial structure parameters.

Indices	Formula	Value				
		0	(0,0.25]	(0.25,0.5]	(0.5,0.75]	(0.75,1]
U	$U_i = \frac{1}{n}\sum_{j=1}^{n} k_{ij}$ $t_{ij} = \begin{cases} 1\ if\ H_i < H_j \\ 0\ if\ H_i > H_j \end{cases}$	superior	sub-superior	moderation	disadvantage	absolute disadvantage

Table A2. *Cont.*

Indices	Formula	Value				
		0	**(0,0.25]**	**(0.25,0.5]**	**(0.5,0.75]**	**(0.75,1]**
UCI	$UCI_i = \frac{U_i}{180 \times n} \sum_{j=1}^{n} (\alpha_1 + \alpha_2)$ $\alpha_1 = \begin{cases} \arctan\left(\frac{H_i}{d_{ij}}\right) \times \frac{180}{\pi} \text{ When } H_j > H_i; \\ \arctan\left(\frac{H_j}{d_{ij}}\right) \times \frac{180}{\pi} \quad \text{Otherwise.} \end{cases}$ $\alpha_2 = \begin{cases} \arctan\left(\frac{H_i - H_j}{d_{ij}}\right) \times \frac{180}{\pi} \text{ When } H_j > H_i; \\ 0 \quad \text{Otherwise.} \end{cases}$	no pressure	less pressure	medium pressure	greater pressure	great pressure
OP	$OP_i = \frac{1}{n} \sum_{j=1}^{n} t_{ij}$ $t_{ij} = \begin{cases} 1 \; if \; d_{ij} > \left\lvert H_i - H_j \right\rvert \\ 0 \; if \; d_{ij} \leq \left\lvert H_i - H_j \right\rvert \end{cases}$	completely occluded	occluded	medium open	open	extremely open
W	$W_i = \frac{1}{n} \sum_{j=1}^{n} t_{ij}$ $t_{ij} = \begin{cases} 1 \; a_{ij} < a_0 \\ 0 \; a_{ij} \geq a_0 \end{cases}; \; a_0 = \frac{360}{n+1}$	absolute uniform	uniform	random	aggregation	cluster distributions
S	$S_i = \frac{Z_i}{3} \times \frac{1}{n} \sum_{j=1}^{n} t_{ij}$ $t_{ij} = \begin{cases} 1 & \text{When i and j belong to the same forest layer} \\ 0 & \text{Otherwise.} \end{cases}$	single	slightly simple	medium	slightly complex	complex
K	$K_i = \frac{1}{n} \sum_{j=1}^{n} \frac{d_{ij}}{H_{ij}}$	Value				
		(0,0.2]	(0.2,0.3]	(0.3,0.4]	(0.4,0.5]	(0.5,+∞)
		serious insufficiency	insufficiency	basic sufficiency	sufficient	more than sufficient

Note: i represents the central tree, and j represents the neighboring tree; H_i is the height of the tree i, H_j is the height of the tree j, d_{ij} is the distance between the central tree i and the neighboring tree j, t_{ij} is a discrete variable, a_{ij} represents the minimum angle between i and j, a_0 represents the standard angle, n represents the number of neighboring trees in the center tree i, and z_i represents the number of forest layers in the structural unit where the center tree i is located.

References

1. Wang, Y.; Deng, X.; Zhang, X.; Xiao, F.; Zheng, R.; Yang, B.; Xiang, W. Variations of monthly radial growth of Chinese fir [*Cunninghamia lanceolata* (Lamb.) Hook.] considering its responses to climatic factors. *Eur. J. For. Res.* **2024**, *143*, 1525–1539. [CrossRef]
2. Zhang, X.; Cao, Q.V.; Wang, H.; Duan, A.; Zhang, J. Projecting Stand Survival and Basal Area Based on a Self-Thinning Model for Chinese Fir Plantations. *For. Sci.* **2020**, *66*, 361–370. [CrossRef]
3. Jactel, H.; Nicoll, B.C.; Branco, M.; Gonzalez-Olabarria, J.R.; Grodzki, W.; Långström, B.; Moreira, F.; Netherer, S.; Orazio, C.; Piou, D.; et al. The influences of forest stand management on biotic and abiotic risks of damage. *Ann. For. Sci.* **2009**, *66*, 701. [CrossRef]
4. Bianchi, S.; Huuskonen, S.; Hynynen, J.; Niemistö, P. Comparing wood production and carbon sequestration after extreme thinnings in boreal Scots pine stands. *For. Ecol. Manag.* **2024**, *553*, 121641. [CrossRef]
5. Kang, H.; Seely, B.; Wang, G.; Innes, J.; Zheng, D.; Chen, P.; Wang, T.; Li, Q. Evaluating management tradeoffs between economic fiber production and other ecosystem services in a Chinese-fir dominated forest plantation in Fujian Province. *Sci. Total Environ.* **2016**, *557–558*, 80–90. [CrossRef]
6. Graz, F.P. The behaviour of the measure of surround in relation to the diameter and spatial structure of a forest stand. *Eur. J. For. Res.* **2008**, *127*, 165–171. [CrossRef]
7. Hong, L.; Duan, G.; Fu, S.; Fu, L.; Ma, L.; Li, X.; Fu, J. Response of Stand Spatial Structure to Nitrogen Addition in Deciduous Broad-Leaved Forest in Jigong Mountain. *Sustainability* **2024**, *16*, 5137. [CrossRef]
8. Ali, A.; Poudel, T.R.; Ismail, M.J.; Saha, S.; Dong, L. Associations between stand spatial structures and carbon sequestration on natural Larix gmelinii forests in Northeast China. *Trees For. People* **2025**, *20*, 100837. [CrossRef]
9. Li, T.; Wu, Y.; Ren, F.; Tian, L.; Li, M. Assessing the impact of stand structure on forest net primary productivity: A multiple machine learning-SHAP models and DSEM integrated approach. *Comput. Electron. Agric.* **2025**, *236*, 110427. [CrossRef]
10. Yang, B.; Ma, R.; Zhai, J.; Du, J.; Bai, J.; Zhang, W. Stand spatial structure is more important than species diversity in enhancing the carbon sink of fragile natural secondary forest. *Ecol. Indic.* **2024**, *158*, 111449. [CrossRef]
11. Chen, Y.; Shao, X.; Wang, S.; Jiang, Y.; Zang, L.; Zhang, G.; Liu, Q.; Chen, D.; Ding, F.; Sui, M. How does the water use efficiency of keystone species act on the stand spatial structure and species diversity in a water-scarce karst forest? *Ecol. Indic.* **2025**, *174*, 113444. [CrossRef]
12. Wen, G.; Ma, J.; Xu, W.; Wang, J.; He, W.; Wang, Y.; Wang, X.; Li, T.; Ye, M.; Chen, G.; et al. Response of understory plant functional groups to changes in stand spatial structure in Masson pine (*Pinus massoniana* Lamb.) plantations depends on thinning mode and intensity. *J. Environ. Manag.* **2025**, *376*, 124441. [CrossRef]
13. Ye, S.; Zheng, Z.; Diao, Z.; Ding, G.; Bao, Y.; Liu, Y.; Gao, G. Effects of Thinning on the Spatial Structure of Larix principis-rupprechtii Plantation. *Sustainability* **2018**, *10*, 1250. [CrossRef]
14. Liu, Y.; Wang, X.; He, L.; Liu, Z.; Zeng, X.; Sha, H.; He, B.; Jing, Y.; Li, J.; Chen, J.; et al. Effects of spatial structure on understory vegetation and soil properties in *Pinus tabuliformis* plantation of different succession types in Beijing. *Acta Ecol. Sin.* **2023**, *43*, 1959–1970. [CrossRef]
15. Mao, Y.; Zhang, H.; Wang, R.; Yan, T.; Wei, W.; You, W. Spatial structure characteristics of the main tree species in a mixed broadleaved Korean pine (*Pinus koraiensis*) forest in a mountainous area of eastern Liaoning Province, China. *Chin. J. Appl. Ecol.* **2019**, *30*, 2933–2940.
16. Szwagrzyk, J.; Szewczyk, J.; Maciejewski, Z. Shade-tolerant tree species from temperate forests differ in their competitive abilities: A case study from Roztocze, south-eastern Poland. *For. Ecol. Manag.* **2012**, *282*, 28–35. [CrossRef]
17. Bāders, E.; Jõgiste, K.; Elferts, D.; Vodde, F.; Kiviste, A.; Luguza, S.; Jansons, Ā. Storm legacies shaping post-windthrow forest regeneration: Learnings from spatial indices in unmanaged Norway spruce stands. *Eur. J. For. Res.* **2021**, *140*, 819–833. [CrossRef]
18. Bu, Y.; Li, W.; von Gadow, K.; Wei, J.; Zhao, P.; Yang, Y.; Zhou, C.; Wang, B.; Zhao, X. Toward a better understanding of forest spatial patterns: A generalisation of the uniform angle index. *Ecol. Model.* **2025**, *503*, 111070. [CrossRef]
19. Zhang, X.; Zhou, C.; Zhang, Z.; Feng, L.; Wang, L.; Fu, L.; Tan, B. Structural Characteristics and Cutting Optimization Model of Larix principis-rupprechtii Plantation in Chongli Winter Olympics Core Area. *Sci. Silvae Sin.* **2022**, *58*, 79–88.
20. Zhao, W.; Cao, X.; Xie, Z.; Pang, Y.; Sun, Y.; Li, J.; Mo, Y.; Yuan, D. Evaluation of Stand Spatial Structure of *Cunninghamia lanceolata* Public Welfare Forest by Using Structural Equation Model. *Sci. Silvae Sin.* **2022**, *58*, 76–88.
21. Wang, Y.; Li, J.; Cao, X.; Liu, Z.; Lv, Y. The Multivariate Distribution of Stand Spatial Structure and Tree Size Indices Using Neighborhood-Based Variables in Coniferous and Broad Mixed Forest. *Forests* **2023**, *14*, 2228. [CrossRef]
22. Li, Y.; He, J.A.; Yu, S.; Wang, H.; Ye, S. Spatial structures of different-sized tree species in a secondary forest in the early succession stage. *Eur. J. For. Res.* **2020**, *139*, 709–719. [CrossRef]
23. Xia, Y.; Shao, D.; Wu, D. Temporal-spatial characteristics of park green space spatial structure and competitive relationship: A multidimensional perspective based on stand spatial structure. *J. Environ. Manag.* **2025**, *380*, 125002. [CrossRef]
24. Dong, L.; Bettinger, P.; Liu, Z. Stand spatial structural diversity: Developing and validating a novel index. *For. Ecol. Manag.* **2024**, *569*, 122157. [CrossRef]

25. Hartley, R.J.L.; Leonardo, E.M.; Massam, P.; Watt, M.S.; Estarija, H.J.; Wright, L.; Melia, N.; Pearse, G.D. An Assessment of High-Density UAV Point Clouds for the Measurement of Young Forestry Trials. *Remote Sens.* **2020**, *12*, 4039. [CrossRef]
26. Oddi, L.; Cremonese, E.; Ascari, L.; Filippa, G.; Galvagno, M.; Serafino, D.; Cella, U.M.D. Using UAV Imagery to Detect and Map Woody Species Encroachment in a Subalpine Grassland: Advantages and Limits. *Remote Sens.* **2021**, *13*, 1239. [CrossRef]
27. Ota, T.; Ogawa, M.; Mizoue, N.; Fukumoto, K.; Yoshida, S. Forest Structure Estimation from a UAV-Based Photogrammetric Point Cloud in Managed Temperate Coniferous Forests. *Forests* **2017**, *8*, 343. [CrossRef]
28. Neuville, R.; Bates, J.S.; Jonard, F. Estimating Forest Structure from UAV-Mounted LiDAR Point Cloud Using Machine Learning. *Remote Sens.* **2021**, *13*, 352. [CrossRef]
29. Castilla, G.; Filiatrault, M.; McDermid, G.J.; Gartrell, M. Estimating Individual Conifer Seedling Height Using Drone-Based Image Point Clouds. *Forests* **2020**, *11*, 924. [CrossRef]
30. Hu, X.; Li, D. Research on a Single-Tree Point Cloud Segmentation Method Based on UAV Tilt Photography and Deep Learning Algorithm. *IEEE J. Sel. Top. Appl. Earth Obs. Remote Sens.* **2020**, *13*, 4111–4120. [CrossRef]
31. Yu, S.; Chen, X.; Huang, X.; Chen, Y.; Hu, Z.; Liu, J.; Yu, K. Research on the Estimation of Chinese Fir Stand Volume Based on UAV-LiDAR Technology. *Forests* **2023**, *14*, 1252. [CrossRef]
32. Hu, Z.; Shan, L.; Chen, X.; Yu, K.; Liu, J. Individual Tree Segmentation of UAV-LiDAR Based on the Combination of CHM and DSM. *Sci. Silvae Sin.* **2024**, *60*, 14–24.
33. You, H.; Liu, Y.; Lei, P.; Qin, Z.; You, Q. Segmentation of individual mangrove trees using UAV-based LiDAR data. *Ecol. Inform.* **2023**, *77*, 102200. [CrossRef]
34. Chen, X.; Yu, K.; Yu, S.; Hu, Z.; Tan, H.; Chen, Y.; Huang, X.; Liu, J. Study on Single-Tree Segmentation of Chinese Fir Plantations Using Coupled Local Maximum and Height-Weighted Improved K-Means Algorithm. *Forests* **2023**, *14*, 2130. [CrossRef]
35. He, X.; Wang, R.; Feng, C.; Zhou, X. A Novel Type of Boundary Extraction Method and Its Statistical Improvement for Unorganized Point Clouds Based on Concurrent Delaunay Triangular Meshes. *Sensors* **2023**, *23*, 1915. [CrossRef] [PubMed]
36. Zhang, C.; Li, J.; Cao, X.; Zhao, C.; Li, J. Analysis on spatial structure of Cunninghamia lanceolata non-commerciaforest based on weighted Voronoi diagram. *J. Cent. South Univ. For. Technol.* **2015**, *35*, 19–26.
37. Cao, X.; Li, J.; Hu, Y.; Yang, J. Spatial structure optimizing model of stand thinning of *Cunninghamia lanceolata* ecological forest. *Chin. J. Ecol.* **2017**, *36*, 1134–1141.
38. Cao, X.; Li, J.; Wei, X. Effects of Spatial Structure on Soil Nutrient Content in Typical Forests in the Contral-Subtropics of China. *Sci. Silvae Sin.* **2020**, *56*, 20–28.
39. Zhou, C.; Zhang, H.; Xu, Q.; Lei, X. Analysis of inter-layer structure based on the relationship of neighboring trees. *J. Beijing For. Univ.* **2019**, *41*, 66–75.
40. Wang, Y.; Wang, D.; Wang, Y.; Yun, H.; Zhang, M.; Zhang, Y. Effects of density and spatial structure of middle-aged *Robinia preudoacacia* plantations on the diversity of shrub and grass in the Loess Plateau. *Acta Ecol. Sin.* **2025**, *45*, 822–836.
41. Li, J.; Liu, S.; Zhang, H.; Kuang, Z.; Wang, C.; Zhang, J.; Cao, X. Heterogeneity evaluation of forest ecological system spatial structure in Dongting Lake. *Acta Ecol. Sin.* **2013**, *33*, 3732–3741. [CrossRef]
42. Huang, S.; Wang, H.; Peng, H.; Wang, Y.; Li, Y.; Ye, S. Analysis of Second-Order Characteristics of Tree Species Dominance in an Old GrowthForest Community in Yachang Nature Reserve. *Sci. Silvae Sin.* **2022**, *58*, 128–140.
43. Chen, K.; Zhang, H.; Lei, X.; Lou, M.; Wang, Q.; Mao, J. Effect of Thinning on Spatial Structure of Spruce-fir Mixed Broadleaf-conifer Forest Base on Crop Tree Management. *For. Res.* **2017**, *30*, 718–726.
44. Na, W.; Zhao, Z.C. The comprehensive evaluation method of low-carbon campus based on analytic hierarchy process and weights of entropy. *Environ. Dev. Sustain.* **2021**, *23*, 9308–9319. [CrossRef]
45. Liang, H.; Wu, M.; Jia, X.; Yang, Q. Comprehensive Evaluation of Soil Improvement Benefits of Biological Retention Facilities Based on AHP-CRITIC. *Buildings* **2024**, *14*, 780. [CrossRef]
46. Zhu, S.; Guo, L.; Cui, Y.; Xiao, R.; Yu, Z.; Jin, Y.; Fu, R.; Zhang, J.; Xu, T.; Chen, J.; et al. Quality suitability modeling of volatile oil in Chinese Materia Medica—Based on maximum entropy and independent weight coefficient method: Case studies of Atractylodes lancea, Angelica sinensis, Curcuma longa and *Atractylodes macrocephala*. *Ind. Crop. Prod.* **2019**, *142*, 111807. [CrossRef]
47. Wang, M.W.; Wang, Y.; Shen, F.Q.; Jin, J.L. Projection Pursuit Method Based on Connection Cloud Model for Assessment of Debris Flow Disasters. *J. Environ. Inform.* **2022**, *41*, 118–129. [CrossRef]
48. Peng, J.; Zhang, J. Urban flooding risk assessment based on GIS- game theory combination weight: A case study of Zhengzhou City. *Int. J. Disaster Risk Reduct.* **2022**, *77*, 103080. [CrossRef]
49. Lyu, C.; Zhang, H.X.; Liu, S.; Guo, Y. Fishing capacity evaluation of fishing vessel based on cloud model. *Sci. Rep.* **2022**, *12*, 8976. [CrossRef]
50. Li, L.; Wei, L.; Li, N.; Zhang, S.; Wu, Z.; Dong, M.; Chen, Y. Extracting the DBH of Moso Bamboo Forests Using LiDAR: Parameter Optimization and Accuracy Evaluation. *Forests* **2024**, *15*, 804. [CrossRef]
51. Ye, N.; Mason, E.; Xu, C.; Morgenroth, J. Estimating individual tree DBH and biomass of durable Eucalyptus using UAV LiDAR. *Ecol. Inform.* **2025**, *89*, 103169. [CrossRef]

52. Konôpka, B.; Pajtík, J.; Marušák, R.; Bošeľa, M.; Lukac, M. Specific leaf area and leaf area index in developing stands of Fagus sylvatica L. and Picea abies Karst. *For. Ecol. Manag.* **2016**, *364*, 52–59. [CrossRef]
53. Owen, H.J.F.; Flynn, W.R.M.; Lines, E.R. Competitive drivers of interspecific deviations of crown morphology from theoretical predictions measured with Terrestrial Laser Scanning. *J. Ecol.* **2021**, *109*, 2612–2628. [CrossRef]
54. Li, Z.; Gao, C.; Che, F.; Li, J.; Wang, L.; Cui, K. Trunk distortion weakens the tree productivity revealed by half-sib progeny determination of Pinus yunnanensis. *BMC Plant Biol.* **2024**, *24*, 629. [CrossRef] [PubMed]
55. Zhang, S.; Fu, B.; Gao, E.; Jia, M.; Sun, W.; Wu, Y.; Zhou, G. Combining UAV-LiDAR point clouds and SSAFormer algorithms for classification of mangrove communities. *Natl. Remote Sens. Bull.* **2025**, *29*, 1140–1163. [CrossRef]
56. Yan, Y.; Lei, J.; Jin, J.; Shi, S.; Huang, Y. Unmanned Aerial Vehicle–Light Detection and Ranging-Based Individual Tree Segmentation in Eucalyptus spp. Forests: Performance and Sensitivity. *Forests* **2024**, *15*, 209. [CrossRef]
57. McAlhaney, A.L.; Keim, R.F.; Allen, S.T. Species-specific growth capacity for floodplain forest trees inferred from sapwood efficiency and individual tree competition. *For. Ecol. Manag.* **2020**, *476*, 118427. [CrossRef]
58. Tetemke, B.A.; Birhane, E.; Rannestad, M.M.; Eid, T. Competition and slope effect on wood basic density and its variation among tree species and within individual trees in a dry Afromontane Forest. *For. Sci. Technol.* **2024**, *20*, 349–360. [CrossRef]
59. He, L.; Zhu, T.; Wu, Y.; Li, W.; Zhang, H.; Zhang, X.; Cao, T.; Ni, L.; Hilt, S. Littoral Slope, Water Depth and Alternative Response Strategies to Light Attenuation Shape the Distribution of Submerged Macrophytes in a Mesotrophic Lake. *Front. Plant Sci.* **2019**, *10*, 169. [CrossRef]
60. Kumar, R.; Singh, S.; Bilga, P.S.; Jatin; Singh, J.; Singh, S.; Scutaru, M.; Pruncu, C.I. Revealing the benefits of entropy weights method for multi-objective optimization in machining operations: A critical review. *J. Mater. Res. Technol.* **2021**, *10*, 1471–1492. [CrossRef]
61. Jiang, X.; Chen, X.; Jiao, Y.; Zhang, L. Objective Evaluation of Motion Cueing Algorithms for Vehicle Driving Simulator Based on Criteria Importance through Intercriteria Correlation (CRITIC) Weight Method Combined with Gray Correlation Analysis. *Machines* **2024**, *12*, 344. [CrossRef]
62. Wu, H.; Zang, L.; Xiao, B.; Liu, Y.; Wang, X.; Guo, X. Evaluation of Driving Behavior Economy Based on Big Data of New Energy Bus. *China J. Highw. Transp.* **2022**, *25*, 177–190.
63. Xu, F.; Wang, K.; Liu, Z. Attribute interval recognition model based on projection pursuit weight for evaluation of stability of surrounding rock. *Rock Soil Mech.* **2010**, *31*, 2587–2591, 2598.
64. Li, Y.; Hu, Z. A tri-system urban waterlogging risk assessment framework based on GIS- game theory combination weight: A case of Zhengzhou City. *Nat. Hazards* **2024**, *120*, 14649–14681. [CrossRef]
65. Yang, Z.; Huang, X.; Fang, G.; Ye, J.; Lu, C. Benefit evaluation of East Route Project of South to North Water Transfer based on trapezoid cloud model. *Agric. Water Manag.* **2021**, *254*, 106960. [CrossRef]
66. Yang, J.; Wan, Q.; Han, J.; Xing, S. An evaluation model for automobile intelligent cockpit comfort based on improved combination weighting-cloud model. *PLoS ONE* **2023**, *18*, e0282602. [CrossRef] [PubMed]
67. Ma, Z.; Zhang, S. Risk-Based Multi-Attribute Decision-Making for Normal Cloud Model Considering Pre-Evaluation Information. *IEEE Access* **2020**, *8*, 153891–153904. [CrossRef]
68. Zhang, W.; Tian, Y.; Yang, Y.; Zhang, P.; Gu, J.; Yang, L.; Jiang, Y.; Zhang, K.; Wang, L. Multiple distribution of spatial structure parameters and tree competition of Larix gmelinii forest stand. *J. Cent. South Univ. For. Technol.* **2025**, *45*, 74–81.
69. Guo, W.; Zhang, Q.; Wang, C.; Wang, Y. Effect of forest management on the secondary forest vegetation carbon density and its distribution in Northeast of China. *Acta Ecol. Sin.* **2024**, *44*, 8651–8660.
70. Wu, S.; Cao, X.; Yan, W.; Yuan, D.; Zhang, Z.; Wang, M.; Huang, X.; Xiang, Y. Spatial structure and soil nutrient characteristics of Cunninghamia lanceolata forest of different age groups and their correlations. *J. Cent. South Univ. For. Technol.* **2025**, *45*, 115–122.
71. Yao, L.; Wang, Z.; Wu, C.; Yuan, W.; Zhu, J.; Jiao, J.; Jiang, B. Competition and Facilitation Co-Regulate Spatial Patterns and Coexistence in a Coniferous and Broad-Leaved Mixed Forest Community in Zhejiang, China. *Forests* **2022**, *13*, 1356. [CrossRef]
72. Cao, Y.; Ye, S.; Zhang, C.; Zhou, W.; Ning, C. Spatial Structure of Forest Stand and Intra-specific Competition in the Cunninghamia lanceolata Plantation in Da-tong Mountain. *J. Northeast. For. Univ.* **2024**, *52*, 8–12, 18.
73. Zhu, J.; Li, X.; Liu, Y.; Chai, Z. Evaluation of Spatial Structure and Dynamic Analysis of Pinus massoniana Plantation. *J. West China For. Sci.* **2025**, *54*, 9–17.
74. Reynolds, J.H.; Ford, E.D. Improving competition representation in theoretical models of self-thinning: A critical review. *J. Ecol.* **2005**, *93*, 362–372. [CrossRef]
75. Zhang, M.; Luo, Y.; Wang, S.; Zhang, L.; Ma, C.; Yu, S.; Wang, J. Spatial Structure Analysis and Optimization of Larix principis-rupprechtii Plantation in Wangyedian, Inner Mongolia. *J. Northwest For. Univ.* **2024**, *39*, 81–87, 107.

Disclaimer/Publisher's Note: The statements, opinions and data contained in all publications are solely those of the individual author(s) and contributor(s) and not of MDPI and/or the editor(s). MDPI and/or the editor(s) disclaim responsibility for any injury to people or property resulting from any ideas, methods, instructions or products referred to in the content.